UNIVERSITAT DE
BARCELONA

Universitat de Barcelona

—

Thesis for the Master of Nuclear physics

THE DOUBLE STRANGENESS PENTAQUARK AND OTHER EXOTIC HADRONS IN THE REACTION $\Xi_B \to J/\Psi\Phi\Xi$

Josep Arnau Marsé i Valera
arnaumv23@gmail.com

Supervisor(s): Àngels Ramos and Volodymyr Magas

26/06/2022

Abstract

We study the possibility that four Ξ *resonances* ($\Xi(1620)$, $\Xi(1690)$, $\Xi(1820)$, $\Xi(1950)$) *could correspond to pentaquark states, in the form of a meson-baryon bound systems. We also explore the possible existence of doubly strange pentaquarks with hidden charm* (P_{css}) *and find two candidates structured in a similar form, at energies of* 4493 MeV *and* 4630 MeV. *The meson-baryon interaction is built from t-channel meson exchange processes which are evaluated using effective Lagrangians. Moreover we analyse the* $\Xi_b \to \Xi\ J/\psi\ \phi$ *decay process, which permits exploring the existence of the heavy double strange pentaquark, as well as other exotic hadrons, in the three different two-body invariant mass spectra of the emitted particles. In the* $J/\psi\phi$ *mass spectrum, we analyse the nature of the* $X(4140)$ *and* $X(4160)$ *resonances. In the* $J/\psi\Xi$ *invariant mass spectrum, we study the signal produced by the doubly strange pentaquark, where we conclude that it has a good chance to be detected in this reaction if its mass is around* $4580 - 4680$ MeV. *Finally, in the* $\phi\Xi$ *spectrum we study the likelihood to detect the* $\Xi(2500)$ *state.*

Contents

List of Figures

List of Tables

1. Introduction

In the last few decades lots of different multi-quark states have been observed experimentally, showing the existence of more complex structures than the conventional mesons and baryons, made of a quark-antiquark pair and three quarks respectively. This fact motivated many theoretical groups to study models that can generate hadrons beyond the standard structures, which increased our understanding of the hadron interaction. One kind of these exotic configurations proposes baryons composed by five quarks, but structured in a quasi-bound state of an interacting meson-baryon pair. One example of the success of this type of models is provided by the $\Lambda(1405)$ resonance, for which the quarks models systematically over-predicted its mass. Instead, dedicated studies of the meson-baryon interaction obtained from chiral effective Lagrangians predict the $\Lambda(1405)$ to be a $\bar{K}N$ molecule [1–3]. After the successful interpretation of the $\Lambda(1405)$, many groups tried to extend this kind of models to other spin, isospin and flavour sectors, finding a more natural way to explain different states, like the $f_0(500)$ and the $a_0(980)$, which are described as meson-meson quasi-bound states [4–6].

More resent experimental results, like the discovery at LHCb [7,8] of four excited resonances of the nucleon ($P_c(4312)$, $P_c(4380)$, $P_c(4440)$ and $P_c(4457)$) seen on the invariant mass distribution of $J/\psi p$ pairs from the Λ_b decay, and the more recent report of LHCb [9] which, analysing the Ξ_b decay finds evidence of the existence of a pentaquark with strangeness ($P_{cs}(4459)$) on the invariant mass distribution of $J/\psi\Lambda$ pairs, clearly establish the need for including a $c\bar{c}$ pair excitation, in order to reproduce the high masses of these states. Baryons with hidden charm, structured as a meson-baryon molecule, had been predicted in some earlier works [10–14], but the existence of a hidden charm pentaquark with double strangeness was not obtained. A recent work studying hadronic molecules states of a baryon with charm and a meson with an anti-charm finds that the bound energy for the $\Xi_c'\bar{D}_s^*$ pair is positive, pointing that the pentaquark with double strangeness may exist [15]. If this state exists it should be visible on the $\eta_c\Xi$ or $J/\psi\Xi$ invariant mass spectrum.

Other examples of exotic states are the X meson resonances. There is still a discussion of the nature and properties of the $X(4140)$ and $X(4160)$ states. In 2008, the Belle collaboration reported the existence of the $X(4160)$ [16] in the $e^-e^+ \to J/\psi D^*\bar{D}^*$ reaction and, during the following years, some groups reported the existence of a narrow $X(4140)$ with a width around 19 MeV [17–22]. Despite of these results, a more recent measurement of the $B^+ \to J/\psi\phi K^+$ decay from the LHCb collaboration [23] obtained a width of 83 MeV for $X(4140)$, which is pretty large compared with the previously studies. In that work other states that couple to $J/\psi\phi$ were also reported such as the $X(4274)$, $X(4550)$ and the $X(4700)$, but the $X(4160)$, which is the state that was previously seen in 2008, was not observed. It might be that the reason of this large width for $X(4140)$ is related to the fact that the two neighbouring states (the narrow $X(4140)$ state plus rather $X(4160)$ resonance) were fitted together. In this work we will study the interplay between the $X(4140)$ and the $X(4160)$ resonances and will try to find an observable that permit us to discriminate whether the truly nature of this state is only one wide $X(4140)$ resonance or it is the combination of a narrow $X(4140)$ state plus a $X(4160)$ one.

Among the theoretical works studying these X states, there were some groups trying to identify the $X(4140)$ as a molecular state of a $D_s^*\bar{D}_s^*$ pair with the quantum numbers 0^{++} and 2^{++} [24–26], but these studies did not take into account the light meson states, producing a small width for the state, hence it was associated to the $X(4140)$. Later, in Ref. [27], the contribution of the light meson channels were included, generating a 2^{++} X state at 4169 MeV with a width of 139 MeV that strongly couples to $D_s^*\bar{D}_s^*$ and it was associated to the $X(4160)$. In the end the quantum numbers of $X(4140)$ were measured, obtaining that these were 1^{++} [28], therefore the models that predict this state as a $D_s^*\bar{D}_s^*$ molecule are no longer supported.

The purpose of the $\Xi_b \to \Xi\ J/\psi\ \phi$ decay studied in this work is to show that in the two-body invariant mass distributions of the three possible pair of particles ($J/\psi\phi$, $J/\psi\Xi$, $\phi\Xi$) there exists a good possibility to detect exotic hadrons. These kind of decays ($A \to a\ b\ c$) had already been used to detect new exotic states, such as the four P_c states or the most recent P_{cs}.

From the relativistic kinematics of a three body decay the Dalitz plot can be generated, which represents the available invariant mass for the different pairs of particles. So if we explore the Dalitz plots for the $\Xi_b \to \Xi\ J/\psi\ \phi$ reaction (Fig. 1) we can see whether the different exotic resonances lie inside the kinematically allowed region.

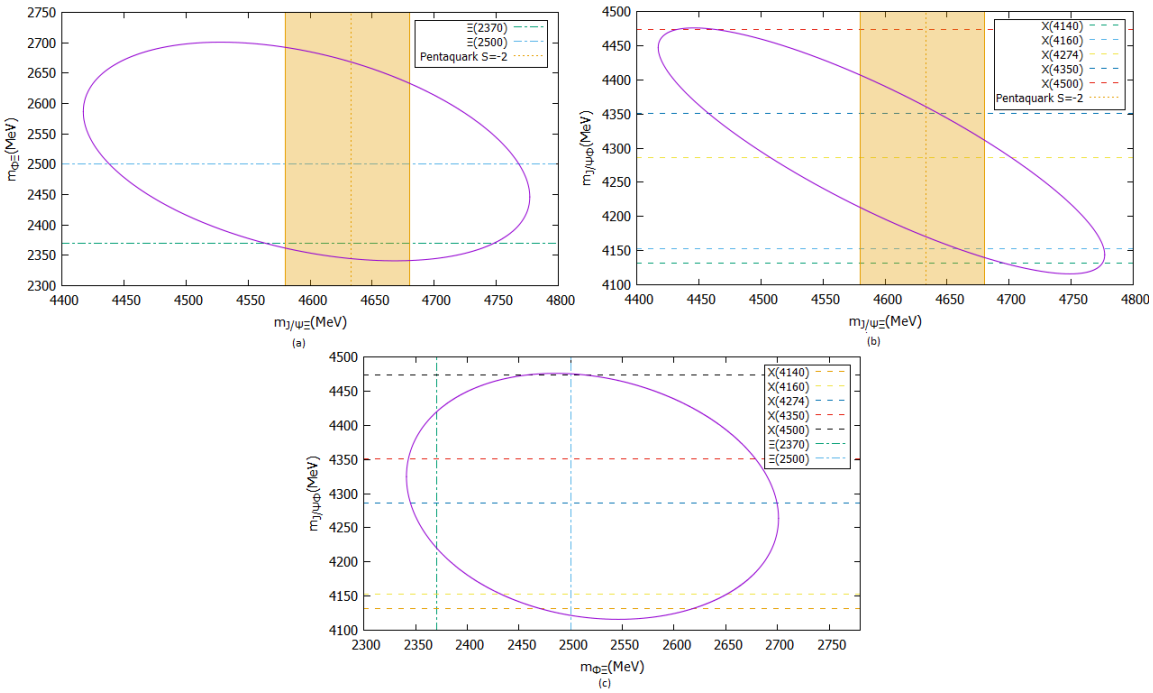

Figure 1: The solid lines represent the Dalitz plot for $M_{\phi\Xi}$ vs $M_{J/\psi\Xi}$ (a), $M_{J/\psi\phi}$ vs $M_{J/\psi\Xi}$ (b) and $M_{J/\psi\phi}$ vs $M_{\phi\Xi}$ (c). The dashed lines show the mass position for different resonances that couple to the corresponding channel. The shadowed zone is the variation we considered in this work for the pentaquark position.

On the $M_{J/\psi\Xi}$ vs $M_{\phi\Xi}$ Dalitz plot (Fig. 1 (a)) the dashed vertical line corresponds to the mass predicted for the $S = -2$ pentaquark and the shadowed zone shows the variations of its mass of $\simeq \pm 50$ MeV due to theoretical uncertainties. We note that, if the pentaquark with double strangeness, disscused later in this work, appears inside the allowed kinematical region, then it may contribute with an important peak in the corresponding invariant mass distribution. In the $M_{J/\psi\Xi}$ vs $M_{J/\psi\phi}$ Dalitz plot (Fig. 1 (b)) five X resonances lie inside the permitted kinematical region, namely the $X(4140)$, $X(4160)$, $X(42740)$, $X(4550)$ and the $X(4700)$. In spite of the fact that all five may be detectable, we will not consider the last tree states since there is at the moment no theoretical model that describes them. Finally, in the $M_{J/\psi\phi}$ vs $M_{\phi\Xi}$ Dalitz plot we can see how we could observe two Ξ resonances in the invariant mass distribution. Since we do not have a theoretical model that describes these two Ξ resonances, we will study the minimal coupling they need to have to produce a visible effect to invariant mass distribution.

2. Formalism

2.1 Meson Baryon states

2.1.1 Meson-Baryon interaction

The model of the meson-baryon interaction used in this work is based on the tree-level diagrams of Fig. 2. In this work we will only consider the s-wave amplitude, for which the most important contribution comes from the t-channel term (Fig. 2(a)). The s- and u- channel terms (Fig. 2(b) and (c)) contribute mostly to the p-wave amplitude and they may have effects at higher energies. In Ref. [29] the contribution from these terms in the $S = -1$ sector were calculated, and were found to be around 20% of that of the dominant t-channel around 200 MeV above the threshold. We can expect that in the sector we study ($S = -2$) these terms will contribute even less, as the intermediate baryon is more massive, and therefore they will be neglected.

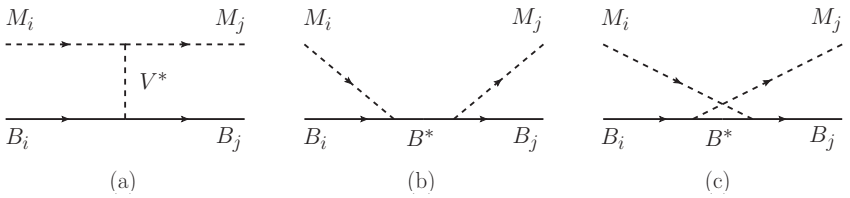

Fig. 2: Leading order tree-level diagrams contributing to the meson-baryon interaction. Baryons and mesons are depicted by solid and dashed lines, respectively.

To describe the interaction we employ effective Lagrangians that describe the couplings of the vector meson to pseudoscalar mesons (VPP) and baryons (VBB), which are obtained using the hidden gauge formalism and assuming $SU(4)$ symmetry [11]:

$$\mathcal{L}_{VPP} = ig\langle [\partial_\mu \phi, \phi]\, V^\mu \rangle, \tag{1}$$

$$\mathcal{L}_{VBB} = \frac{g}{2} \sum_{i,j,k,l=1}^{4} \bar{B}_{ijk}\gamma^\mu \left(V^k_{\mu,l} B^{ijl} + 2V^j_{\mu,l} B^{ilk} \right), \tag{2}$$

where ϕ and V_μ represent the 16-plet pseudo-scalar field and the 16-plet vector field, respectively, and $\langle\ \rangle$ denotes the $SU(4)$ trace in flavour space. The g factor is a coupling constant which is related to the pion decay constant ($f = 93$ MeV) and a representative mass of a light vector meson from nonet (m_V) through the following relation,

$$g = \frac{m_V}{2f}. \tag{3}$$

Using the VPP and VBB vertices in the t-exchange diagram of Fig. 2 (a) one can obtain the s-wave interaction kernel V_{ij} [11] for the pseudoscalar meson baryon (PB) interaction:

$$V_{ij} = g^2 \sum_v C^v_{ij} \bar{u}(p_j)\gamma^\mu u(p_i) \frac{1}{t - m_v^2} \times \left[(k_i + k_j)_\mu - \frac{k_i^2 - k_j^2}{m_v} (k_i + k_j)_\mu \right], \tag{4}$$

where $p_{i/j}$ and $k_{i/j}$ denote the four-momentum of the baryons and mesons, respectively, and i, j are the incoming and outgoing meson-baryon channels. The mass of the vector meson interchanged is m_v, and we approximate it, as $m_v = m_V$, being equal for all of the vector mesons without charm quark and/or antiquark. For the charmed mesons we add a factor $\kappa_c = (m_V/m_V^c)^2 = 1/4$ for D^*, D_s^* mesons and $\kappa_{cc} = 1/9$ for the J/ψ in order to take account of their higher mass. This simplifies Eq. (4) into

$$V_{ij} = -C_{ij} \frac{1}{4f^2} \bar{u}(p_j)\gamma^\mu u(p_i)(k_i + k_j)_\mu, \tag{5}$$

where we have taken the limit where $t \ll m_V$, which reduces the t-channel diagram to a contact term, and we have included the κ_c and κ_{cc} factors in the C_{ij} matrix of coefficients. This expression can be further simplified using the Dirac algebra up to $\mathcal{O}(p^2/M^2)$, what leads to:

$$V_{ij}(\sqrt{s}) = -C_{ij}\frac{1}{4f^2}\left(2\sqrt{s} - M_i - M_j\right)N_i N_j, \tag{6}$$

where M_i, M_j are the masses of the baryons in the channels i and j, N_i and N_j are the normalization factors $N_i = \sqrt{(E_i + M_i)/2M_i}$ and E_i, E_j are the energies of the corresponding baryons. We note that although $SU(4)$ symmetry has been employed to obtain the C_{ij} coefficients, our interaction potential is not $SU(4)$ symmetric, since we use the physical masses of mesons and baryons.

The interaction of vector mesons with baryons is built in a similar way and involves a three-vector VVV vertex obtained from

$$\mathcal{L}_{VVV} = ig\langle[V^\mu, \partial_\nu V_\mu]V^\nu\rangle. \tag{7}$$

One can see that in this case we can arrive to a similar expression as Eq. (6), but multiplied by the product of the polarisation vectors, $\vec{\epsilon}_i \cdot \vec{\epsilon}_j$:

$$V_{ij}(\sqrt{s}) = -C_{ij}\vec{\epsilon}_i \cdot \vec{\epsilon}_j\frac{1}{4f^2}\left(2\sqrt{s} - M_i - M_j\right)N_i N_j. \tag{8}$$

2.1.2 The $I = 1/2$ $S = -2$ sector

For the sector we are studying ($I = 1/2$ $S = -2$) we have 9 possible pseudoscalar-meson baryon channels, $\pi\Xi(1456)$, $\bar{K}\Lambda(1611)$, $\bar{K}\Sigma(1689)$, $\eta\Xi(1866)$, $\eta'\Xi(2276)$, $\eta_c\Xi(4302)$, $\bar{D}_s\Xi_c(4437)$, $\bar{D}_s\Xi_c'(4545)$, $\bar{D}\Omega(4565)$, where the values in parenthesis denote their thresholds. As can be seen, the channels with hidden charm are about 2 GeV more massive compared with the other channels. Therefore we can expect these two regions to be essentially independent, making only a rather small effects on each other. The values of the C_{ij} coefficients for the 9-channels are the ones seen in Table 1.

	$\pi\Xi$	$\bar{K}\Lambda$	$\bar{K}\Sigma$	$\eta\Xi$	$\eta'\Xi$	$\eta_c\Xi$	$\bar{D}_s\Xi_c$	$\bar{D}_s\Xi_c'$	$\bar{D}\Omega_c$
$\pi\Xi$	2	$\frac{3}{2}$	$\frac{1}{2}$	0	0	0	0	0	$\sqrt{\frac{3}{2}}\kappa_c$
$\bar{K}\Lambda$		0	0	$-\frac{3}{2}$	0	0	$-\frac{1}{2}\kappa_c$	$-\frac{\sqrt{3}}{2}\kappa_c$	0
$\bar{K}\Sigma$			2	$\frac{3}{2}$	0	0	$\frac{3}{2}\kappa_c$	$-\frac{\sqrt{3}}{2}\kappa_c$	0
$\eta\Xi$				0	0	0	κ_c	$\frac{1}{\sqrt{3}}\kappa_c$	$\frac{1}{\sqrt{6}}\kappa_c$
$\eta'\Xi$					0	0	$\frac{1}{\sqrt{8}}\kappa_c$	$-\frac{1}{\sqrt{6}}\kappa_c$	$\frac{1}{\sqrt{3}}\kappa_c$
$\eta_c\Xi$						0	$\sqrt{\frac{3}{2}}\kappa_c$	$\frac{1}{\sqrt{2}}\kappa_c$	$-\kappa_c$
$\bar{D}_s\Xi_c$							$-1 + \kappa_{cc}$	0	0
$\bar{D}_s\Xi_c'$								$-1 + \kappa_{cc}$	$\sqrt{2}$
$\bar{D}\Omega_c$									κ_{cc}

Table 1: Coefficients C_{ij} of the PB interaction in the $I = 1/2$, $S = -2$ sector

In the VB sector, the allowed channels are $\rho\Xi(2089)$, $\bar{K}^*\Lambda(2010)$, $\bar{K}^*\Sigma(2087)$, $\omega\Xi(2101)$, $\phi\Xi(2338)$, $J/\psi\Xi(4415)$, $\bar{D}_s^*\Xi_c(4581)$, $\bar{D}_s^*\Xi_c'(4689)$, $\bar{D}^*\Omega(4706)$, where we can again separate the channels in two sets, one with the light channels and the other with the heavy ones. In this case we can obtain the C_{ij} coefficients directly form the those in Table 1 using these following correspondences,

$$\pi \to \rho, \quad K \to K^*, \quad \bar{K} \to \bar{K}^*, \quad D \to D^*, \quad \bar{D} \to \bar{D}^*, \quad \eta_c \to J/\psi$$

$$\tfrac{1}{\sqrt{3}}\eta + \sqrt{\tfrac{2}{3}}\eta' \to \omega \qquad \text{and} \qquad -\sqrt{\tfrac{2}{3}}\eta + \tfrac{1}{\sqrt{3}}\eta' \to \phi\ , \tag{9}$$

	$\rho\Xi$	$\bar{K}^*\Lambda$	$\bar{K}^*\Sigma$	$\omega\Xi$	$\phi\Xi$	$J/\psi\Xi$	$\bar{D}_s^*\Xi_c$	$\bar{D}_s^*\Xi_c'$	$\bar{D}^*\Omega_c$
$\rho\Xi$	2	$\frac{3}{2}$	$\frac{1}{2}$	0	0	0	0	0	$\sqrt{\frac{3}{2}}\kappa_c$
$\bar{K}^*\Lambda$		0	0	$-\frac{\sqrt{3}}{2}$	$\sqrt{\frac{3}{2}}$	0	$-\frac{1}{2}\kappa_c$	$-\frac{\sqrt{3}}{2}\kappa_c$	0
$\bar{K}^*\Sigma$			2	$\frac{\sqrt{3}}{2}$	$-\sqrt{\frac{3}{2}}$	0	$\frac{3}{2}\kappa_c$	$-\frac{\sqrt{3}}{2}\kappa_c$	0
$\omega\Xi$				0	0	0	κ_c	$\frac{1}{\sqrt{3}}\kappa_c$	$\frac{1}{\sqrt{6}}\kappa_c$
$\phi\Xi$					0	0	$\frac{1}{\sqrt{8}}\kappa_c$	$-\frac{1}{\sqrt{6}}\kappa_c$	$\frac{1}{\sqrt{3}}\kappa_c$
$J/\psi\Xi$						0	$\sqrt{\frac{3}{2}}\kappa_c$	$\frac{1}{\sqrt{2}}\kappa_c$	$-\kappa_c$
$\bar{D}_s\Xi_c$							$-1+\kappa_{cc}$	0	0
$\bar{D}_s\Xi_c'$								$-1+\kappa_{cc}$	$\sqrt{2}$
$\bar{D}\Omega_c$									κ_{cc}

Table 2: Coefficients C_{ij} of the VB interaction in the $I = 1/2$, $S = -2$ sector

and are listed in Table 2.

Note that for the light PB sector, due to the fact that all C_{5j} cofficients with $j \leq 5$ are zero, we formally have only 4 coupled channels, while this does not occur for the light VB sector and we have 5 coupled channels in this case.

2.1.3 Resonances

The sought resonances are dynamically generated as poles of the scattering amplitude T_{ij}, which is unitarized via the on-shell Bethe-Salpeter equation in coupled channels. Doing that we implement the resumation of loop diagrams to the infinite order (see Fig. 3),

$$T_{ij} = V_{ij} + V_{il}G_lV_{lj} + V_{il}G_lV_{lk}G_kV_{kj} + ... = V_{ij} + V_{il}G_lT_{lj} \tag{10}$$

where G_l is the loop function, which is given by

$$G_l = i\int \frac{d^4q}{(2\pi)^4}\frac{2M_l}{(P-q)^2 - M_l^2 + i\epsilon}\frac{1}{q^2 - m_l^2 + i\epsilon}, \tag{11}$$

the masses M_l and m_l correspond to those of the baryon and meson of the l channel, respectively, $P = p+k = (\sqrt{s}, 0)$ is the total four momenta in the c.m. frame, and q denotes the four momentum in the intermediate loop. We factorise the V and T matrices on-shell out of the integrals in Eq. (10) [30], hence obtaining the following algebraic matrix expression for the scattering amplitude,

$$T = (1 - VG)^{-1}V. \tag{12}$$

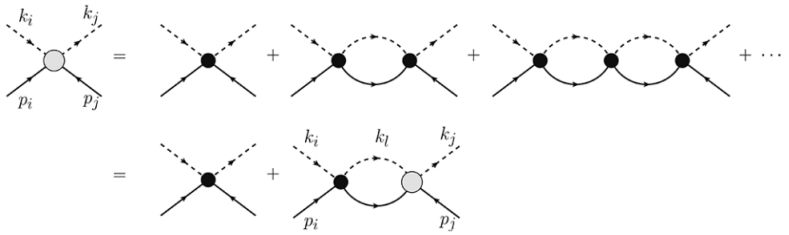

Fig. 3: Diagrams that represent the Bethe-Salpeter equation. The empty circle corresponds to the T_{ij} matrix elements, the black ones represent the V_{ij} potential and the loops are the G_l propagator functions.

Note that the sum over the polarisation vector in the case of the vector meson baryon interaction gives [30]

$$\sum_{pol}\epsilon_i\epsilon_j = \delta_{ij} + \frac{q_iq_j}{M_V^2}, \tag{13}$$

where, consistently with our model, we neglect the q^2/M_V^2 term, thus all $\vec{\epsilon}_i\vec{\epsilon}_j$ factorize out from all terms in the Bethe-Salpeter equation.

It is important to know that the loop function in Eq. (11) diverges logarithmically, so we must renormalize it. We can employ the *cut-off* method, which consists in changing the infinity at the upper limit to one large enough cut-off momentum Λ

$$G_l^{\rm cut} = \int d\Omega_q \int_0^{\Lambda} \frac{q^2 dq}{(2\pi)^3} \frac{1}{2\omega_l(\vec{q}\,)} \frac{M_l}{E_l(\vec{q}\,)} \frac{1}{\sqrt{s} - \omega_l(\vec{q}\,) - E_l(\vec{q}\,) + i\epsilon}, \tag{14}$$

The disadvantage of this model is that such a model is not valid for energies higher than

$$m \sim \sqrt{m_{\rm bar}^2 + \Lambda^2} + \sqrt{m_{\rm mes}^2 + \Lambda^2}. \tag{15}$$

A different option is using the *dimensional regularisation* scheme, which gives rise to the following analytic expression

$$\begin{aligned} G_l = & \frac{2M_l}{16\pi^2}\Big\{ a_l(\mu) + \ln\frac{M_l^2}{\mu^2} + \frac{m_l^2 - M_l^2 + s}{2s}\ln\frac{m_l^2}{M_l^2} + \\ & + \frac{q_l}{\sqrt{s}}\Big[\ln\left(s - (M_l^2 - m_l^2) + 2q_l\sqrt{s}\right) \\ & \quad + \ln\left(s + (M_l^2 - m_l^2) + 2q_l\sqrt{s}\right) \\ & \quad - \ln\left(-s + (M_l^2 - m_l^2) + 2q_l\sqrt{s}\right) \\ & \quad - \ln\left(-s - (M_l^2 - m_l^2) + 2q_l\sqrt{s}\right)\Big]\Big\}, \end{aligned} \tag{16}$$

were q_l is the on-shell three-momentum of the meson in the loop, and we have introduced a subtraction constant, $a(\mu)$, at the regularisation scale μ. In this work we will take $\mu = 1000$ MeV consistently with the previous approaches [30]. The value of the subtraction constant that produces the same loop function at threshold as that obtained with a cut-off Λ is determined by

$$a_l(\mu) = \frac{16\pi^2}{2M_l}\left(G_l^{\rm cut}(\Lambda) - G_l(\mu, a_l = 0)\right). \tag{17}$$

As can be seen, some mesons in the considered channels have with a large width ($\Gamma_\rho = 149.4$ MeV and $\Gamma_{K^*} = 50.5$ MeV), but G_l in Eq. (16) does not take into account this fact. Therefore, in order to implement the meson width we comvolute this function with the mass distribution of the particle. This method has been used in [30,31] and the resulting loop function for these channels becomes:

$$\tilde{G}_l(s) = -\frac{1}{N}\int_{(m_l-2\Gamma_l)^2}^{(m_l+2\Gamma_l)^2} \frac{d\tilde{m}_l^2}{\pi}\,{\rm Im}\,\frac{1}{\tilde{m}_l^2 - m_l^2 + i\,m_l\Gamma(\tilde{m}_l)} \times G_l\left(s, \tilde{m}_l^2, M_l^2\right), \tag{18}$$

where we extend the integration limits up to twice the meson width on either side of the mass, and the normalisation factor N is

$$N = \int_{(m_l-2\Gamma_l)^2}^{(m_l+2\Gamma_l)^2} d\tilde{m}_l^2 \left(-\frac{1}{\pi}\right) {\rm Im}\,\frac{1}{\tilde{m}_l^2 - m_l^2 + i\,m_l\Gamma(\tilde{m}_l)}\ . \tag{19}$$

The energy-dependent width is given by

$$\Gamma(\tilde{m}_l) = \Gamma_l \frac{m_l^5}{\tilde{m}_l^5}\frac{\lambda^{3/2}(\tilde{m}_l^2, m_1^2, m_2^2)}{\lambda^{3/2}(m_l^2, m_1^2, m_2^2)}\,\theta(\tilde{m}_l - m_1 - m_2), \tag{20}$$

where m_1 and m_2 are the masses of the lighter mesons into which the vector meson decays and λ is the Källén function $\lambda(x,y,z) = (x - (\sqrt{y} + \sqrt{z})^2)(x - (\sqrt{y} - \sqrt{z})^2)$.

The resonances are generated as poles of the scattering amplitude T_{ij} in the so-called *second Riemann sheet*, obtained by using the following rotation of the loop function:

$$G_l^{\rm II}(\sqrt{s}+i\epsilon) = G_l(\sqrt{s}+i\epsilon) + i\frac{q_l}{4\pi\sqrt{2}}. \tag{21}$$

Around the pole, the scattering amplitude can be approximated as

$$T_{ij} \simeq \frac{g_i g_j}{z - z_p}, \tag{22}$$

from which we can obtain the coupling constants, g_i, of the resonance for all channels. In addition, we calculate the compositeness defined as:

$$\chi_i = \left| g_i^2 \frac{\partial G_i(z_p)}{\partial z} \right|, \tag{23}$$

which approximately gives the contribution of the i-th channel meson-baryon component in a given resonance.

2.2 The $\Xi_b \to \Xi\ J/\psi\ \phi$ decay

2.2.1 Primary decay

Studying the $\Xi_b \to \Xi X \to \Xi\ J/\psi\ \phi$ decay we, apart from the search for the double strangeness pentaquark, have also a chance to study the interplay between the $X(4140)$ and $X(4160)$ resonances. Similar to what was done in Refs. [32, 33], we use two independent primary decay mechanisms, one for $X(4160)$ and other for $X(4140)$. Since for the $X(4140)$ resonance we do not have a physical model to generate it, we introduce it as a Breit-Wigner whose parameters are fitted to experimental data. While the $X(4160)$ can be obtained as a result of chiral unitarized coupled-channels calculation (Ref. [27]), i.e. as a meson-meson molecule resonance strongly coupled to $D_s^*\bar{D}_s^*$ channel.

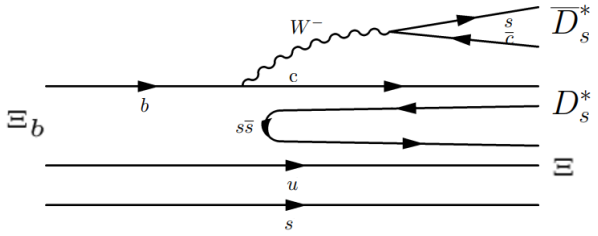

Fig. 4: Microscopic quark level $\Xi_b \to \Xi\ D_s^*\ \bar{D}_s^*$ transition, through internal emission.

Let us start with the $\Xi_b \to \Xi\ J/\psi\ \phi$ decay via $X(4160)$ production. Since the $X(4160)$ strongly couples to the $D_s^*\ \bar{D}_s^*$ channel (Fig. 4), we can start considering the $\Xi_b \to \Xi D_s^*\ \bar{D}_s^*$ weak decay mechanism. Then, as shown in Fig. 5, the $D_s^*\ \bar{D}_s^*$ lines form a loop, allowing multiple couple channel interactions and generating dynamically the $X(4160)$, which then decay into J/ψ and ϕ. The amplitude of this process can be written as:

$$\mathcal{M}^P_{X_{4160}} = A(\vec{\epsilon}_{J/\psi} \times \vec{\epsilon}_\phi) \cdot \vec{P}_\Xi G_{D_s^*\bar{D}_s^*} \frac{T_{D_s^*\bar{D}_s^*, J/\psi\phi}}{g_{D_s^*\bar{D}_s^*} g_{J/\psi\phi}}. \tag{24}$$

The A on the right side of the equation represents the strength of the $\Xi_b \to \Xi D_s^*\ \bar{D}_s^*$ weak decay, represented in Fig. 4, which we are not going to study in details. This value can be taken as a constant due to the limited range of energies involved in the $\Xi_b \to \Xi\ J/\psi\ \phi$ decay as it is argued

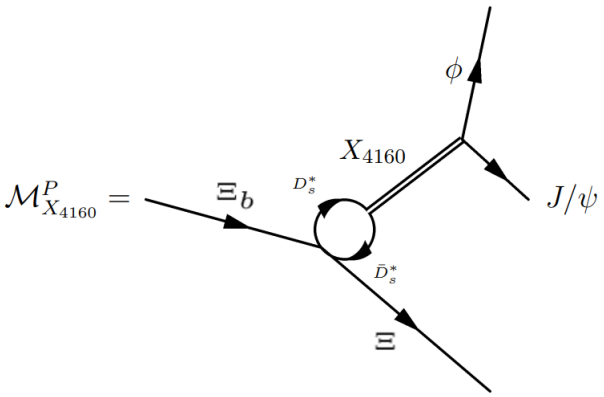

Fig. 5: Mechanism for the $\Xi_b \to J/\psi\ \phi\ \Xi$ decay involving the $X(4160)$ resonance.

in Ref. [34]. The $(\vec{\epsilon}_{J/\psi} \times \vec{\epsilon}_{\phi}) \cdot \vec{P}_{\Xi}$ factor denotes the P-wave operator which is the minimum partial wave we need in the weak vertex to conserve the angular momentum, since the spins of Ξ_b and Ξ is $J = 1/2$ meanwhile for the $X(4160)$ are $J = 2$. Here the ϵ_i represents the polarisation of the vector mesons in the $J/\psi\ \phi$ rest frame and $\vec{P}_{\Xi}$ the tree-momentum of the Ξ in the same frame. The factor $G_{D_s^* \bar{D}_s^*}$ indicates the contribution of the $D_s^* \bar{D}_s^*$ loop shown in Fig. 5 and the $T_{D_s^* \bar{D}_s^*, J/\psi\phi}$ term is the coupled-channel unitarized amplitude for the $D_s^* \bar{D}_s^* \to J/\psi\ \phi$ process. Note that we divide it by the corresponding couplings constants, this is done to simplify the comparison with the $X(4140)$ term.

Now we will discus the $X(4140)$ production process which is shown in Fig. 6 and and the associated amplitude is

$$\mathcal{M}^P_{X_{4140}} = \frac{\tilde{B}}{2M_{X(4140)}[M_{J/\psi\phi} - M_{X(4140)} + i\frac{\Gamma_{X(4140)}}{2}]}, \tag{25}$$

where the $X(4140)$ is parameterised with a Breit-Wigner, where $M_{J/\psi\phi}$ is the invariant mass of the $J/\psi\phi$ system and $M_{X(4140)}$ and $\Gamma_{X(4140)}$ are the mass and width of $X(4140)$ resonance, respectively. A new constant connected to the strength of the $\Xi_b \to \Xi\ X(4140)$ weak decay is B, and since we need to have the same units for the strength parameters of different reactions to compare them, we have introduced $\tilde{B}$ via the following relation, $\tilde{B} = BM_{X(4140)}$. Now A and $\tilde{B}$ have the same units and can be compared. In this process we do not need to have a P-vertex since the quantum number of the $X(4140)$ is $J = 1$, therefore the minimum partial wave needed to conserve the angular momentum is $L = 0$.

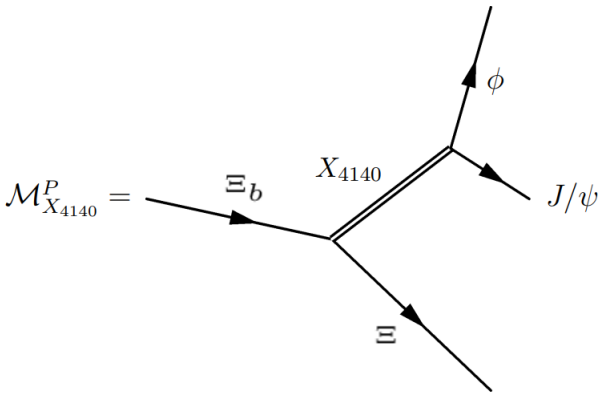

Fig. 6: Mechanism for the $\Xi_b \to J/\psi\ \phi\ \Xi$ decay involving the $X(4140)$ resonance

We will not go into more detailed calculations, since the main aim of this work is to point out

the possibility to use the $\Xi_b \to \Xi\ J/\psi\ \phi$ decay to study already discovered and and potentially possible exotic states and to encourage to the experimental collaborations to explore this reaction.

2.2.2 Final state interaction

Once we discussed the generation of the $\Xi\ J/\psi\ \phi$ final state in Ξ_b decay we want to focus on studying the final state interaction in the $\Xi\ J/\psi$ and $\Xi\ \phi$ channels. For the case of the final state interaction of $\Xi\ J/\psi$ pair the Ξ and J/ψ legs from Fig. 5 and 6 have to be closed, forming a loop, which can dynamically generate the $S = -2$ pentaquark. The $\Xi\ \phi$ final state interaction can produce excited Ξ states and has to be studied in a similar way.

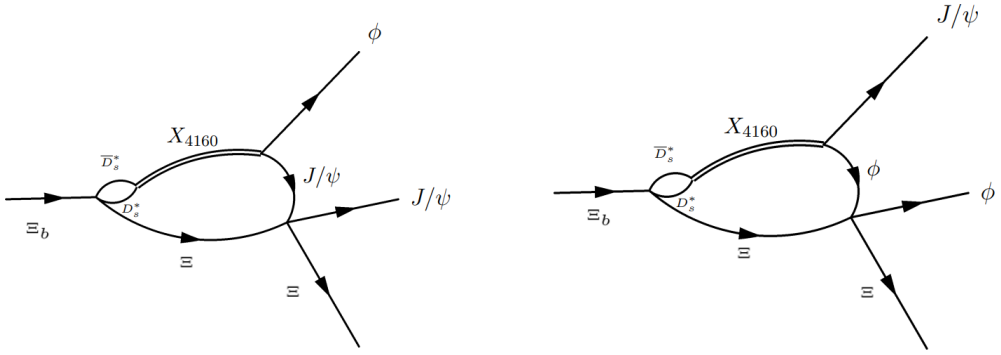

Fig. 7: Final state interaction between $J/\psi\ \Xi$ (a) and $\phi\ \Xi$ (b) in the presence of the $X(4160)$ resonance.

The amplitude associated to the process with the final state interaction of the $J/\psi\Xi$ pair driven by the Ξ_b decay via $X(4160)$ resonance is:

$$\mathcal{M}^{J/\psi\Xi}_{X_{4160}} = A(\vec{\epsilon}_{J/\psi} \times \vec{\epsilon}_{\phi}) \cdot \left(\frac{\vec{P}_\Xi - \vec{P}_\phi}{2}\right) T_{J/\psi\Xi, J/\psi\Xi} I^{J/\psi\Xi}_{X_{4160}}, \tag{26}$$

which is associated to the diagram shown in Fig. 7(a), where the superscript denotes the final state interaction channel. This expression is derived in the Appendix A, and the expression for the integral $I^{J/\psi\Xi}_{X_{4160}}$ is also given. We would like to remind the reader that for the decay via $X(4160)$ the weak decay vertex has to be a P-wave one. Therefore the operator assigned to the the $\Xi_b \to D_s^*\ \bar{D}_s^*\ \Xi$ is proportional to the momentum of Ξ and the loop integral (Fig. 7(a)) becomes a tree-vector. To evaluate this loop integral we use the $J/\psi\ \Xi$ rest frame, where the loop became proportional to $(\vec{P}_\Xi - \vec{P}_\phi)$ times an scalar loop $\left(I^{J/\psi\Xi}_{X_{4160}}\right)$. The term $T_{J/\psi\Xi, J/\psi\Xi}$ captures the final state interaction contribution from $J/\psi\ \Xi$, which in this work we will model using Breit-Wigner form:

$$T_{J/\psi\Xi, J/\psi\Xi} = \frac{g^2_{J/\psi\ \Xi}}{M_{J/\psi\ \Xi} - M + i\frac{\Gamma}{2}}, \tag{27}$$

were $g_{J/\psi\ \Xi}$ is the coupling of the $S = -2$ pentaquark to the $J/\psi\ \Xi$ channel. $M_{J/\psi\ \Xi}$ denotes the invariant mass of the $J/\psi\ \Xi$ system and the M and Γ factors represents the mass and the width of the $S = -2$ pentaquark. $g_{J/\psi\ \Xi}$, M, Γ will be obtained from the molecular model of a vector meson interacting with a baryon explained in the section 2.1.

For the final state interaction of the $\phi\ \Xi$ pair we can repeat similar calculations and obtain (see Appendix A):

$$\mathcal{M}^{\phi\Xi}_{X_{4160}} = A(\vec{\epsilon}_{J/\psi} \times \vec{\epsilon}_{\phi}) \cdot \left(\frac{\vec{P}_\Xi + \vec{P}_\phi}{2}\right) T_{\phi\Xi, \phi\Xi} I^{\phi\Xi}_{X_{4160}} \tag{28}$$

where the $T_{\phi\Xi,\phi\Xi}$ factor also has a Breit-Wigner form, as in the Eq. (27), but in this case M and Γ are the experimental mass and width of $\Xi(2500)$. Since we do not have any model which can give us the value of $g_{\phi\Xi}$, we will invert the problem and will study for which values of $g_{\phi\Xi}$ it is feasible to see this state using the $\Xi_b \to \Xi\ J/\psi\ \phi$ reaction.

Now we go to the final states interaction in the presence of the $X(4140)$ resonance. The corresponding diagrams are given in Figs. 8(a) and 8(b) and the associated analytical expressions are

$$\mathcal{M}^{J/\psi\Xi}_{X_{4140}} = \tilde{B} T_{J/\psi\Xi,J/\psi\Xi} I^{J/\psi\Xi}_{X_{4140}}, \tag{29}$$

$$\mathcal{M}^{\phi\Xi}_{X_{4140}} = \tilde{B} T_{\phi\Xi,\phi\Xi} I^{\phi\Xi}_{X_{4140}}. \tag{30}$$

These expressions are explained in more detail in Appendix A. The terms $I^{J/\psi\Xi}_{X_{4140}}$ and $I^{\phi\Xi}_{X_{4140}}$ are scalar loop integral analogous to those in Eqs. 26 and 28.

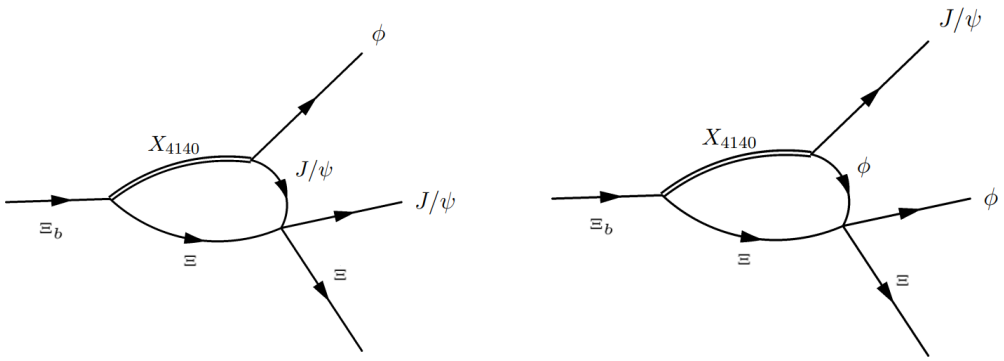

Fig. 8: Final state interaction between $J/\psi\ \Xi$ (a) and $\phi\ \Xi$ (b) in the presence of the $X(4140)$ resonance.

2.2.3 Full amplitude

Now we proceed to combine the various terms to form the full invariant amplitude. Firstly we put together the $X(4140)$ terms into a $\mathcal{M}_{X_{4140}}$ amplitude, and similarly for $X(4160)$ terms,

$$\mathcal{M}_{X_{4140}} = \mathcal{M}^{P}_{X_{4140}} + \mathcal{M}^{J/\psi\Xi}_{X_{4140}} + \mathcal{M}^{\phi\Xi}_{X_{4140}}, \tag{31}$$

$$\mathcal{M}_{X_{4160}} = \mathcal{M}^{P}_{X_{4160}} + \mathcal{M}^{J/\psi\Xi}_{X_{4160}} + \mathcal{M}^{\phi\Xi}_{X_{4160}}. \tag{32}$$

We also implement this useful re-definition,

$$\mathcal{M}_{4140} \to \tilde{B}\mathcal{M}_{4140}, \tag{33}$$

$$\mathcal{M}_{4160} \to A\mathcal{M}_{4160}. \tag{34}$$

Finally we mix this terms obtaining the full amplitude denoted as $\mathcal{M}$,

$$\overline{\mathcal{M}} = |A|^2\overline{|\mathcal{M}_{4160}|^2} + |\tilde{B}|^2\overline{|\mathcal{M}_{4140}|^2} = |A|^2\Big(\overline{|\mathcal{M}_{4160}|^2} + |\beta|\overline{|\mathcal{M}_{4140}|^2}\Big). \tag{35}$$

where the bar represents the sum over polarisations and $\beta = |\tilde{B}|^2/|A|^2$. Note that since the weak decay goes in P-wave for the $X(4160)$ contribution, and in S-wave for the $X(4140)$ contributions, this cancels the cross term in $\overline{|\mathcal{M}_{4160} + \mathcal{M}_{4140}|^2}$ as these two partial waves are orthogonal and do not interfere. It is also important to comment that although the the overall factor $|A|^2$ is not known, it is not relevant for our shape obtained distributions. The form of the distributions, and

not its absolute value, will be our main observable, for example, the position of the peak and it width can be measured even in such a situation. So our final results will be given in arbitrary units, therefore we will set it as $|A|^2 = 1$ from here to the end of this work.

The β acts like a relative weight between the $X(4140)$ and $X(4160)$. In this work we will not calculate its value and we do not have any experimental result to compare it, so we take the value of β from the Ref. [33] to solve this issue. In this reference the authors study the interplay between $X(4160)$ and $X(4140)$ in the $B^+ \to J/\psi\ \phi\ K^+$ decay. The mechanism involving the $X(4160)$ in this reaction is rather similar at the quark level to our diagram shown in Fig. 4, but without the spectator s quark in the initial and final state. Hence the topology of the diagrams is similar also in the case of $X(4140)$. Therefore the β value at our reaction may have a similar value, but we do not expect it to be the exactly the same, since the partial waves involved in the their weak decay vertex are P-wave and D-wave for the $X(4140)$ and $X(4160)$ resonances respectively.

Finally, we explain how we deal with the sum over the polarisations appearing in Eq. (35). For the $\mathcal{M}_{X(4140)}$ this calculation is trivial and it only produces a constant, which can be reabsorbed into β, but for the $\mathcal{M}_{X(4160)}$ amplitude the calculation are more complicated adding cross term contributions. The full derivaton is presented in the Appendix B.

First of all, we introduce the following definitions:

$$\mathcal{M}^{P}_{4160} = (\vec{\epsilon}_{J/\psi} \times \vec{\epsilon}_{\phi}) \cdot \vec{P}_{\Xi}\ \tilde{\mathcal{M}}^{P}_{4160}, \tag{36}$$

$$\mathcal{M}^{J/\psi\Xi}_{4160} = (\vec{\epsilon}_{J/\psi} \times \vec{\epsilon}_{\phi}) \cdot \vec{K}_{2}\ \tilde{\mathcal{M}}^{J/\psi\Xi}_{4160}, \tag{37}$$

$$\mathcal{M}^{\phi\Xi}_{4160} = (\vec{\epsilon}_{J/\psi} \times \vec{\epsilon}_{\phi}) \cdot \vec{K}_{1}\ \tilde{\mathcal{M}}^{\phi\Xi}_{4160}, \tag{38}$$

where $\vec{K}_1 \equiv (\vec{P}_{\Xi} + \vec{P}_{\phi})/2$ and $\vec{K}_2 \equiv (\vec{P}_{\Xi} - \vec{P}_{\phi})/2$. Then, we shown (in Appendix B) that the sum over the polarisations leads to

$$\begin{aligned}\overline{|\mathcal{M}_{4160}|^2} = \quad & |\vec{P}_{\Xi}|^2|\tilde{\mathcal{M}}^{P}_{4160}|^2 + |\vec{K}_2|^2|\tilde{\mathcal{M}}^{J/\psi\Xi}_{4160}|^2 + |\vec{K}_1|^2|\tilde{\mathcal{M}}^{\phi\Xi}_{4160}|^2 + 2\vec{P}_{\Xi}\cdot\vec{K}_2\Re(\tilde{\mathcal{M}}^{P}_{4160}\tilde{\mathcal{M}}^{*J/\psi\Xi}_{4160}) \\ & +2\vec{P}_{\Xi}\cdot\vec{K}_1\Re(\tilde{\mathcal{M}}^{P}_{4160}\tilde{\mathcal{M}}^{*\phi\Xi}_{4160}) + 2\vec{K}_1\cdot\vec{K}_2\Re(\tilde{\mathcal{M}}^{J/\psi}_{4160}\tilde{\mathcal{M}}^{*\phi\Xi}_{4160}),\end{aligned} \tag{39}$$

where $\Re$ is the real part of the complex argument.

3. Results

3.1 Molecular resonances

3.1.1 Light sector

We fist start the discussion with the results for the light channels for the pseudoscalar meson baryon interaction, where we employ the dimensional regularization model to compute the loop function. The first calculations are done employing values of subtractions constants which are determined by imposing the loop function to coincide, for a regularization scale of $\mu = 1000$ MeV, with to the loop function computed with the cut-off scheme with $\Lambda = 800$ MeV at the corresponding threshold (Eq. (17)). We chose this value as it corresponds to the mass of the interchanged vector meson on the t-channel diagram which is integrated out when we take the $t \to 0$ limit. Will refer to this procedure as Model PB 1. The resulting amplitude are shown in Fig. 9, where we represent $\sum_j |T_{ij}|$ as a function of the c.m. energy for all different i channels in different colours. There amplitudes show a board peak (barely visible) at low energies and a narrower one right below the $\bar{K}\Sigma$ threshold. This behaviour is the reflection of two poles, which have the properties shown in Table 3). Note that these states have a well defined spin-parity of $J^\pi = \frac{1}{2}^-$, since they are formed with a scalar meson ($J^\pi = 0^-$) and a baryon ($J^\pi = \frac{1}{2}^+$) interacting in s-wave ($L = 0$).

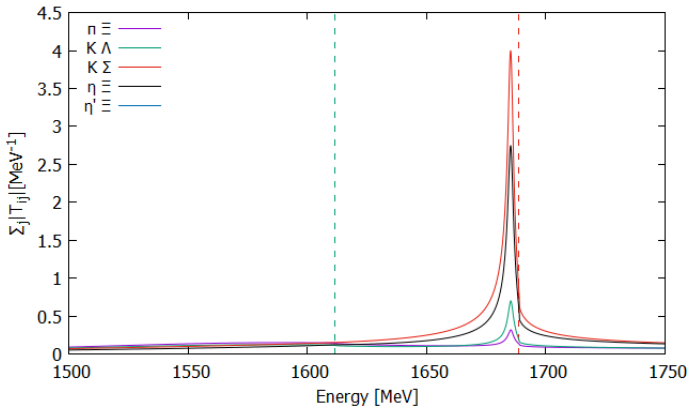

Fig. 9: Solid lines represent the sum over all j channels of the modulus of the PB scattering amplitude, $|T_{ij}|$ for a fixed channel i, obtained using the dimensional regularisation scheme to compute the loop function. The vertical dashed lines represent the location of the thresholds of the different channels.

We can observe how the lowest energy state couples strongly to the $\pi\Xi$ and $\bar{K}\Lambda$ channels, which are open for decay, explaining the large width of this resonance. On the PDG [35] one can find a state with similar mass which was weakly seen in the $\pi\Xi$ channel (Tab. 4). Even if our state is 50 MeV lighter and its width is larger we can see the potential of our model to generate a state in this region. As seen in Table 3 the heavy state mostly couples to the $\bar{K}\Sigma$ and $\eta\Xi$ channels and it has a mass of 1685 MeV. In PDG data there exists a Ξ state at 1690 ± 10 MeV with a width of 20 ± 15 MeV which is compatible with our results.

Looking at the results, it is natural to think that we can modify the values of the subtraction constants within a reasonable range in order to accommodate the generated states to the experimental data. Therefore, we relax the condition of the loop function to be equal, at the corresponding threshold, to the cut-off loop function with $\Lambda = 800$ MeV [30]. By doing that we define a the model, PB 2, in which the light resonance appears in a higher energy region and is much wider, see Table 3, while the heavier resonance is generated with a similar mass and with a slightly larger width. Looking at Table 4 we can see how now the mass of the light state is closer to the experimental energy of the $\Xi(1620)$. In this model, none of the equivalents, cut-off values for the subtractions constants employed are smaller than $\Lambda = 630$ MeV, which is a reasonable value.

$0^- \oplus \frac{1}{2}^+$ interaction in the $(I,S) = (\frac{1}{2}, -2)$ sector						
Model PB 1						
M(Mev)			1570.53		1685.18	
Γ(MeV)			174.04		2.28	
	a_i	Λ	$\lvert g_i\rvert$	χ_i	$\lvert g_i\rvert$	χ_i
$\pi\Xi(1456)$	-1.51	800	2.44	0.428	0.12	0.001
$\bar{K}\Lambda(1611)$	-1.32	800	1.91	0.169	0.27	0.006
$\bar{K}\Sigma(1689)$	-1.27	800	0.71	0.016	1.54	0.815
$\eta\Xi(1866)$	-1.47	800	0.49	0.004	1.06	0.029
Model PB 2						
M(Mev)			1600.55		1685.40	
Γ(MeV)			228.64		2.60	
	a_i	Λ	$\lvert g_i\rvert$	χ_i	$\lvert g_i\rvert$	χ_i
$\pi\Xi(1456)$	-1.30	630	2.70	0.501	0.15	0.001
$\bar{K}\Lambda(1611)$	-1.00	740	2.21	0.214	0.27	0.006
$\bar{K}\Sigma(1689)$	-1.27	800	0.86	0.025	1.53	0.822
$\eta\Xi(1866)$	-1.47	800	0.42	0.003	1.02	0.027

Table 3: Position, subtraction constants, cut off, couplings and compositeness of the Ξ states generated with the light channels of the PB interaction.

PDG data					Model PB 1		Model PB 2	
State	Evidence	J^π	M(MeV)	Γ(MeV)	M(MeV)	Γ(MeV)	M(MeV)	Γ(MeV)
$\Xi(1620)$	*	-	~ 1620	~ 40	1570.53	174.53	1600.55	228.65
$\Xi(1690)$	***	-	1690 ± 10	20 ± 15	1685.18	2.28	1685.40	2.60
PDG					Model VB 2		Model VB 3	
$\Xi(1820)$	***	$\frac{3}{2}^-$	1823 ± 5	24^{+15}_{-10}	1823.12	0.66	–	–
$\Xi(1950)$	***	-	1950 ± 15	60 ± 20	1949.23	0.232	1935.99 1964.09	8.29 4.92

Table 4: Experimental information for the $\Xi(1620)$, $\Xi(1690)$, $\Xi(1820)$, $\Xi(1950)$ resonances and the mass and width for the states generated with four different models.

We proceed now to discuss the results for the vector meson baryon interaction, where we construct the model VB 1 in a similar way as to the model PB 1, i. e. using a regularisation scale of $\mu = 1000$ MeV and imposing that the loop function for each channel has the same value to the one computed with $\Lambda = 800$ MeV at the threshold. Using this model we produce the amplitude displayed in Fig. 10 which have two poles with properties listed in Table 5. Note that each of these states forms a degenerate spin-parity doubled with $J^\pi = \frac{1}{2}^-$, $J^\pi = \frac{3}{2}^-$, since they are produced from the interaction of a vector meson ($J^\pi = 1^-$) an a baryon ($J^\pi = \frac{1}{2}^+$) in the s-wave ($L = 0$).

As it can be seen in Table 5, the light state couples strongly to the $\rho\Xi$ channel. Note that this state, even it has an energy lower that all the thresholds it has a non-zero width. This is because we take into account the width of the ρ and $\bar{K}^*$ in the loop function. For the higher energy peak we can see that it strongly couples to the $\bar{K}^*\Sigma$ channel. On the PDG data one finds two states, the $\Xi(1820)$ and the $\Xi(1950)$. The first state has a known spin-parity $J^\pi = \frac{3}{2}^-$. These quantum numbers are compatible with our model. So similarly at how we did for the PB case, we will modify the subtraction constants within a reasonable range to try to adjust our results to the experimental data.

Modifying the values of the subtraction constants we build model VB 2, which produces two

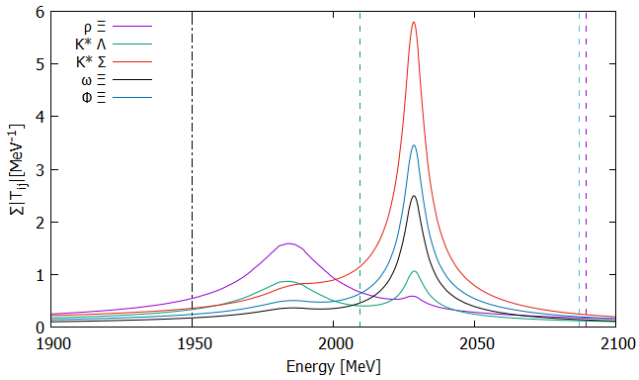

Fig. 10: Solid lines represent the sum over all j channels of the modulus of the PB scattering amplitude, $|T_{ij}|$ for a fixed channel i, obtained using the dimensional regularisation scheme to compute the loop function. The vertical coloured dashed lines represent the location of the thresholds of the different channels and the black one represents the mass position of the $\Xi(1950)$.

$1^- \oplus \frac{1}{2}^+$ interaction in the $(I,S)=(\frac{1}{2},-2)$ sector						
Model VB 1						
M(Mev)			1985.95		2028.40	
Γ(MeV)			29.23		6.86	
	a_i	Λ	$\lvert g_i\rvert$	χ_i	$\lvert g_i\rvert$	χ_i
$\rho\Xi(2089)$	-1.50	800	3.39	0.610	0.24	0.004
$\bar{K}^*\Lambda(2010)$	-1.42	800	1.82	0.358	0.52	0.0490
$\bar{K}^*\Sigma(2087)$	-1.46	800	0.98	0.047	2.97	0.629
$\omega\Xi(2101)$	-1.50	800	0.54	0.014	1.30	0.114
$\phi\Xi(2338)$	-1.57	800	0.75	0.012	1.80	0.077
Model VB 2						
M(Mev)			1823.12		1949.23	
Γ(MeV)			0.66		0.232	
	a_i	Λ	$\lvert g_i\rvert$	χ_i	$\lvert g_i\rvert$	χ_i
$\rho\Xi(2089)$	-2.19	1440	3.48	0.323	0.16	0.001
$\bar{K}^*\Lambda(2010)$	-2.00	1300	2.07	0.131	0.66	0.035
$\bar{K}^*\Sigma(2087)$	-1.87	1140	1.16	0.033	3.15	0.509
$\omega\Xi(2101)$	-1.50	800	0.41	0.004	1.43	0.100
$\phi\Xi(2338)$	-1.80	990	0.56	0.005	1.98	0.100
Model VB 3						
M(Mev)			1935.99		1964.09	
Γ(MeV)			8.29		4.92	
	a_i	Λ	$\lvert g_i\rvert$	χ_i	$\lvert g_i\rvert$	χ_i
$\rho\Xi(2089)$	-1.74	990	2.88	0.335	1.43	0.096
$\bar{K}^*\Lambda(2010)$	-1.42	800	1.41	0.116	1.53	0.186
$\bar{K}^*\Sigma(2087)$	-1.82	1090	2.58	0.250	2.66	0.309
$\omega\Xi(2101)$	-1.50	800	0.41	0.006	1.45	0.092
$\phi\Xi(2338)$	-1.85	1040	0.56	0.006	2.00	0.081

Table 5: Position, subtraction constants, cut off, couplings and compositeness of the Ξ states generated with the light channels of the VB interaction.

resonances at energies compatible with the experimental masses of $\Xi(1829)$ and $\Xi(1950)$ (see Fig. 11 and Table 5), but the width of these states are smaller compared to data. This might be solved if we developed a model which would couple the vector mesons with the pseudoscalar mesons,

as this would open more light channels in which these resonances could decay, increasing their width. The values of the corresponding cut-offs for the subtraction constants are not larger than $\Lambda = 1500$ MeV, which is a reasonable value.

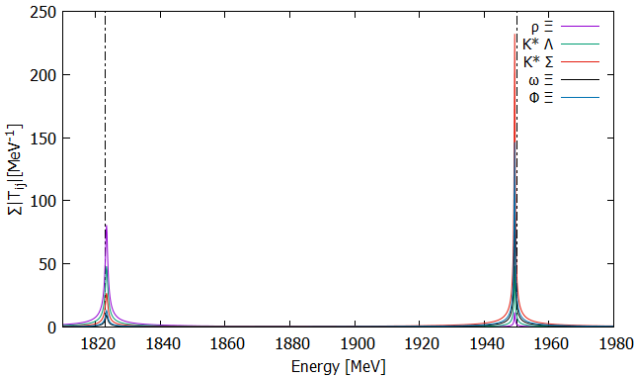

Fig. 11: Solid lines represent the sum over all j channels of the modulus of the PB scattering amplitude, $|T_{ij}|$ for a fixed channel i, obtained using the dimensional regularisation scheme to compute the loop function. The vertical coloured dashed lines represent the location of the thresholds of the different channels and the black one represents the mass position of the $\Xi(1820)$ and the $\Xi(1950)$.

Another possibility to reproduce the experimental data is to generate both resonances in the energy region where $\Xi(1950)$ appears, eventually merging into an apparent wide peak. This is the goal of the model VB 3, which, as seen on Fig. 12 and Table 5, generates two states close to the energy region where the $\Xi(1950)$ appears. Note that for this model we only need to modify tree subtraction constants and the equivalent cut-off values are not larger than 1100 MeV for any channel. As described on the PDG this state could be representing more than one Ξ and, as we show here, this could be a theoretical prediction of model VB 3 if this fact is confirmed.

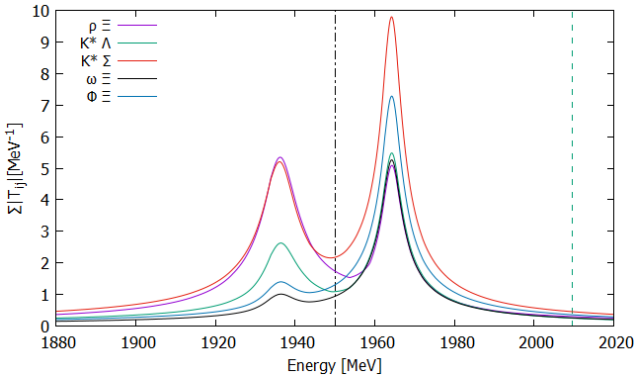

Fig. 12: Solid lines represent the sum over all j channels of the modulus of the PB scattering amplitude, $|T_{ij}|$ for a fixed channel i, obtained using the dimensional regularisation scheme to compute the loop function. The vertical coloured dashed lines represent the location of the thresholds of the different channels and the black one represents the mass position of the $\Xi(1950)$.

3.1.2 Heavy sector

Let's now discus the results for the four heavy channels. We will proceed in a similar way than we did in the previous section. So we first set the regularisation scale to $\mu = 1000$ MeV and the subtraction constants are evaluated for all the channels mapping the loop to the value obtained for a cut-off of $\Lambda = 800$ MeV at the threshold of each channel. Using this model, five peaks are

generated, as we can see in Fig. 13. If we analyse this figure we can see that the four lower energy peaks couple strongly to the $\bar{D}_s\Xi_c$ and $\bar{D}_s\Xi_c'$ channels. However, the diagonal potentials of these channels are repulsive ($C_{ii} < 0$), which is an indication of the fact that these four poles are mathematical artifacts. They appear from Eq. 12 where $VG \simeq 1$ but with a repulsive interaction, which has not physical meaning.

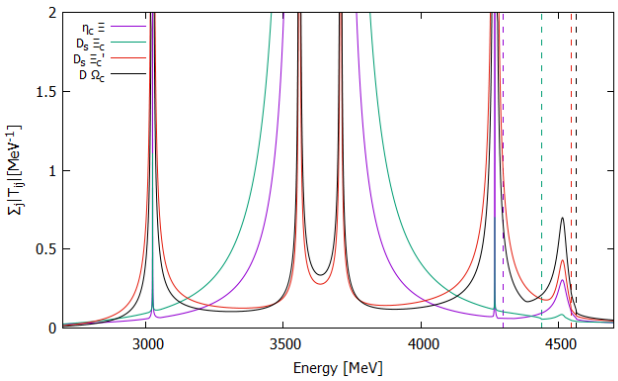

Fig. 13: Solid lines represent the sum over all j channels of the modulus of the PB scattering amplitude, $|T_{ij}|$ for a fixed channel i, obtained using the dimensional regularisation scheme to compute the loop function. The vertical dashed lines represent the location of the thresholds of the different channels.

In order to prove that these states have no physical interpretation we try to find the sign of the diagonal term of the potential (V_{ii}) at the energy where $V_{ii}G_i \simeq 1$. If that is positive, that would mean that we are generating a bound state in a region where the potential is repulsive, which has no physical sense. This is indeed what happens, as can be seen in Fig. 14, where the inverse of the diagonal potential an the dimensional regularisation and cut-off loop functions are represented as function of the c. m. energy for the three different channels. As we can see in Figs. 14(a) and (b) the inverse of the potential and the dimensional regularisation loop almost intersect in a region where the potential is repulsive, denoting to us that the states which mostly couple to $\bar{D}\Xi_c$ and $\bar{D}\Xi_c'$ are only mathematical solutions of our equation but do not represent any physical state.

To avoid the fake pole problem we will now use the cut-off scheme to compute the loop functions, since they are always negative in this scheme, preventing generation of any fake poles. Note that even if the inverse of the diagonal term of the attractive potential and the real part of the loop function are really different on Fig. 14(c), we can still generate an state. This is an effect of the coupled channels as we will show later in this work.

As can be seen in Fig. 15, using a cut-off model with $\Lambda = 800$ MeV, the four fake poles disappear and, as we expected only remains the one at higher energy, which is strongly coupled with the $\bar{D}\Omega_c$ and $\bar{D}_s\Xi_c'$ channels (see Table 6). This state has a well defined spin-parity $J^\pi = \frac{1}{2}^-$ as it is generated from the PB interaction in s-wave.

Comparing our results with other works in the literature using similar models can help us to understand the origin of this state. A resonance which is strongly coupled to the $\bar{D}\Omega_c$ and $\bar{D}_s\Xi_c'$ is also found in Ref. [11], but there the energy at which it is generated is much lower, around 3700 MeV. This huge difference comes from the different renormalisation method used in their work, they force the loop function to be zero at $\mu = \sqrt{m_{th}^2 + M_{th}^2}$, where m_{th} and M_{th} are the masses of the meson and baryon, respectively, of the lightest channel, which this case is $\pi\Xi$. Therefore, we note that we would need a cut-off value of $\Lambda \simeq 2800$ MeV in order to reproduce this behaviour of loop function. Therefore, we can see a clear difference with our work, where we use $\Lambda = 800$ MeV. Such a big value for the cut-off seems unreasonable in our opinion.

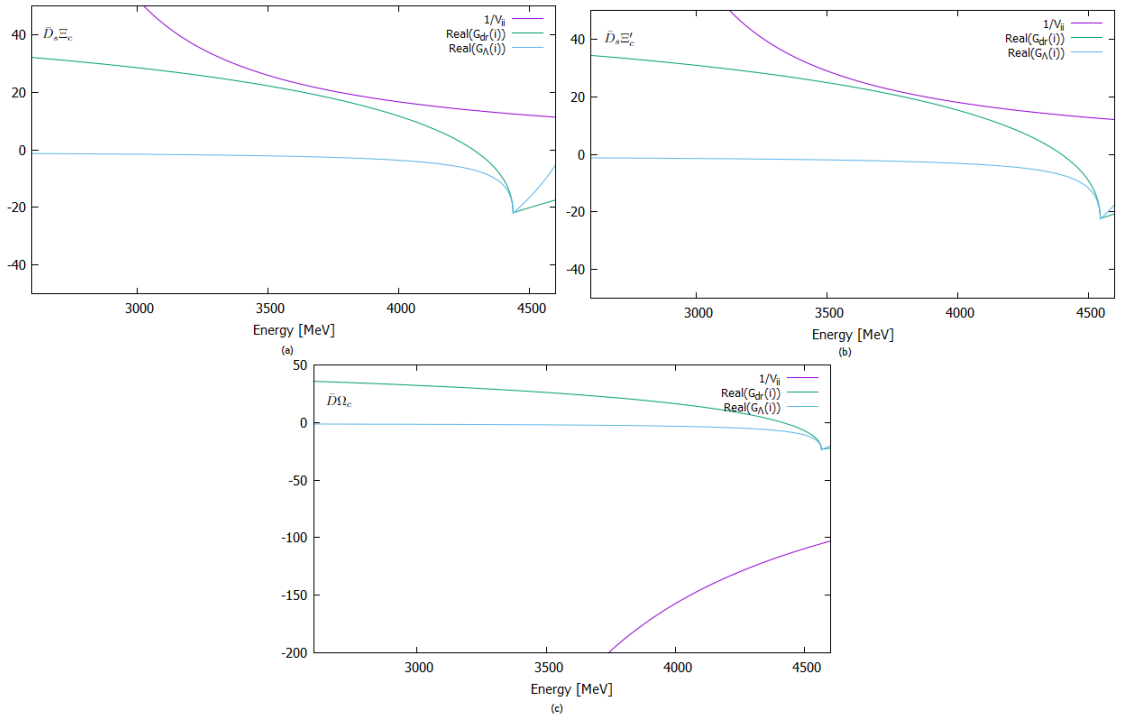

Fig. 14: The purple line represents the inverse of the diagonal term of the potential, the green line shows the loop function of the same channel, computed using a dimensional regularisation scheme, and the blue line is similar to the green one but computed using a cut-off scheme. In (a) we have the $\bar{D}_s\Xi_c$ channel, in (b) the $\bar{D}_s\Xi_c'$ and in (c) the $\bar{D}\Omega_c$

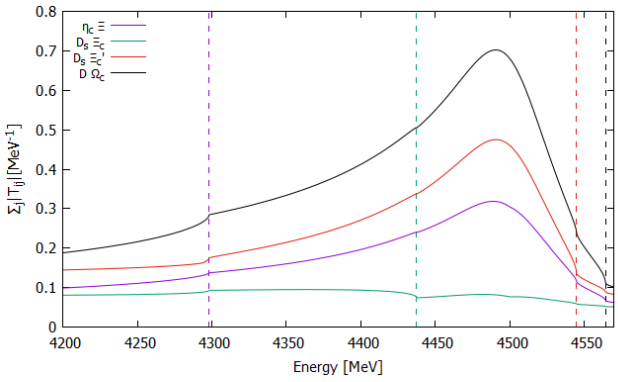

Fig. 15: Solid lines represent the sum over all j channels of the modulus of the PB scattering amplitude, $|T_{ij}|$, obtained using the cut-off model to compute the loop function. The vertical dashed lines represent the location of the thresholds of the different channels.

There are other works, like Ref. [10], that use a more similar way to compute the loop-function, but the state coupling strongly to the $\bar{D}\Omega_c$ and $\bar{D}_s\Xi_c'$ channels is not generated. The main difference with our work is that the authors of Ref. [10] neglect the contribution of κ_{cc}, which is usually a good approximation, since a diagonal term $C_{99} = \kappa_{cc} = 1/9$ is not attractive enough to produce a bound state, as it can be checked using uncoupled channels. But, in this case the non-diagonal terms of the interaction, $C_{98} = -\sqrt{2}$, are strong enough to produce a bound state, via the coupled-channels. To check that we change $C_{89} \to C'_{89} = \gamma C_{89}$, adding a gamma factor which we vary to see how the coupled-channels affect the generation of the resonance. In Fig. 16 we can clearly see the effect of this factor, showing that for small values of gamma ($\gamma \sim 0.5$) the state is not generated.

$0^- \oplus \frac{1}{2}^+$ interaction in the $(I,S)=(0,-2)$ sector				
M(Mev)		4493.35		
Γ(MeV)		73.67		
	Λ	g	$\lvert g_i\rvert$	χ_i
$\eta_c\Xi(4302)$	800	$-1.60+0.34i$	1.63	0.220
$\bar{D}_s\Xi_c(4437)$	800	$-0.17+0.27i$	0.32	0.019
$\bar{D}_s\Xi_c'(4545)$	800	$-2.41+0.58i$	2.48	0.398
$\bar{D}\Omega_c(4564)$	800	$3.59-0.77i$	3.67	0.711

Table 6: Position, cut off, couplings and compositeness of the Ξ state generated with the heavy channels of the PB interaction.

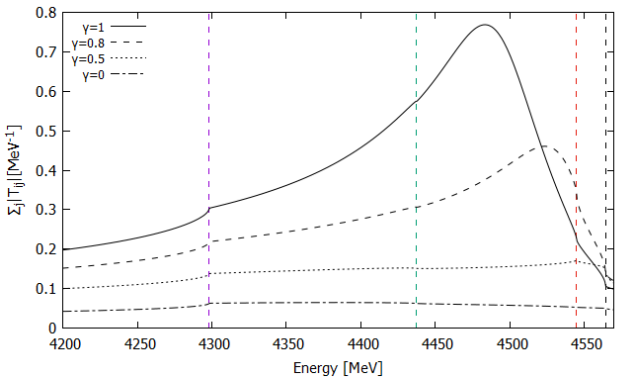

Fig. 16: Solid lines represent the sum over all j channels of the modulus of the PB scattering amplitude, $|T_{ij}|$ for a fixed channel $i=\bar{D}\Omega_c$, obtained using the cut-off scheme to compute the loop function. The vertical dashed lines represent the location of the thresholds of the different channels.

We also want to analyse the influence to our results when we vary the cut-off and we introduce a certain amount of $SU(4)$ symmetry violation associated to the fact that the mass of the charm quark is larger compared to that of the light quarks. Note that we already have introduced $SU(4)$ symmetry violation since we use the physical masses for the meson and baryon in the interaction kernel. So, if we want to introduce an extra 30% of $SU(4)$ symmetry violation and leave the $SU(3)$ symmetry untouched, we can vary the κ_c and κ_{cc} [30] in the range $(1\pm0.3)\kappa_c$ and $(1\pm0.3)\kappa_{cc}$. The gray area in Fig. 17 is the zone in the complex plane where the pole is generated varying the cut-off $\Lambda=750-950$ MeV and introducing a 30% of $SU(4)$ symmetry violation. Note that modifications of the cut-off produces variations in the mass of the resonances, but it slightly affects to its width. By contrary modifications of the $SU(4)$ symmetry breaking produce small changes to the mass of the resonance, but produces important variations on its width.

Modelling an spectrum for this kind of peaks is a difficult task, but we would like to simulate what the experiments would measure. Looking at our peak we see that it only has two open channels, the $\eta_c\Xi$ and $\bar{D}_s\Xi_c$ but since the second one is not strongly coupled to the resonance it will be better seen in the $\eta_c\Xi$ invariant mass spectrum. So to simulate the spectrum, in Fig. 18 we represent the quantity

$$q_{\eta_c}\left|\sum_i T_{i\to\eta_c\Xi}\right|^2 \tag{40}$$

versus the $\eta_c\Xi$ centre-of-mass energy, where $T_{i\to\eta_c\Xi}$ is the scattering amplitude of the $i\to\eta_c\Xi$ transition and we use the η_c momentum in the $\eta_c\Xi$ centre-of-mass energy reference frame, q_{η_c}, as a phase space modulator.

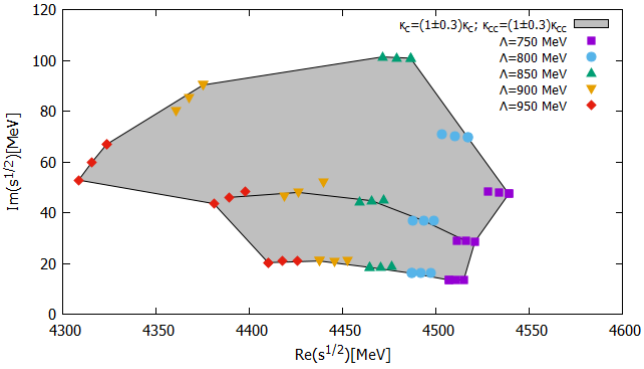

Fig. 17: The symbols indicate the evolution of the pole position of resonance for different cut-off values, represented in the plot by the different colours. For each value of the cut-off, we show $3 \times 3 = 9$ different $SU(4)$ breaking results, corresponding to the possible combinations of the values $(0.7, 1.0, 1.3)\kappa_c$ and $(0.7, 1.0, 1.3)\kappa_{cc}$. The upper dots are obtained with $1.3\kappa_c$ and the lower ones with $0.7\kappa_c$. The black lines are merely to guide the eye and join the results obtained with different cut-off values for the combinations with $1.3\kappa_c$, $0.7\kappa_{cc}$ (upper line), $1.0\kappa_c$, $1.0\kappa_{cc}$ (middle line) and $0.7\kappa_c$, $1.3\kappa_{cc}$ (lower line). The gray area has then to be understood as the region where the pole can be generated assuming up to a 30% breaking of $SU(4)$.

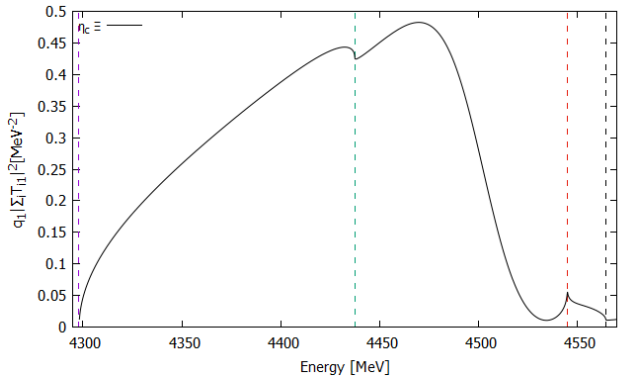

Fig. 18: The solid lines represent the sum of the amplitudes squared times a phase space modulator. The dashed lines represent the thresholds of the different channels.

We now present our results in the heavy VB sector, in this case we proceeding in a similar way as that we did in the PB sector. So we start using the subtraction constants method, also finds five peaks, see Fig. 19. The four at lower energy are fake poles as the dominant channel they couple has a repulsive diagonal potential term. As we did previously, we checle in Fig. 20 if at the energy where $VG \simeq 1$ the potential is repulsive or attractive.

In this sector it is more obvious that the lower energy states are fake poles sine, as can be seen in Fig. 20(a) and (b), the two lines cross twice in a region when the potential is repulsive, indicating that they have no physical meaning. Therefore, as we proceeded in the PB sector, we will now use the cut-off scheme to compute the loop function instead of using the dimensional regularisation one. Note that in Fig. 20(c) now the two lines are closer that in the PB sector which means that it will be easier to generate a state via coupled channels.

Using the cut-off model, as it can be seen in Fig. 21, the four fake poles disappear and it only remains a resonance, which couples strongly to $\bar{D}^*\Omega_c$ and $\bar{D}_s^*\Xi_c'$, see Table 7. Note that this state is degenerate in spin-parity since we have a vector-meson ($J^P = 1^-$) interacting with a baryon ($J^P = \frac{1}{2}^+$) in s-wave ($L = 0$), then it can be $J^P = \frac{1}{2}^-$ or $J^P = \frac{3}{2}^-$.

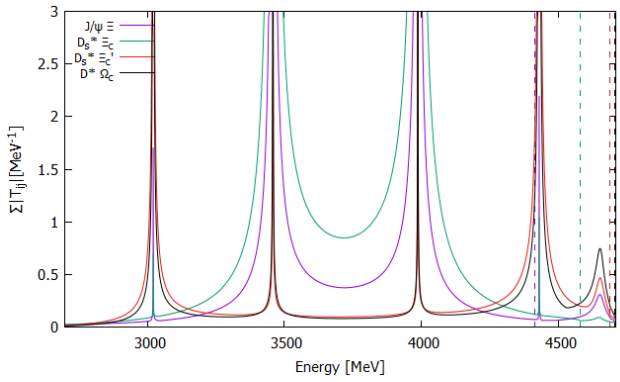

Fig. 19: Solid lines represent the sum over all j channels of the modulus of the VB scattering amplitude, $|T_{ij}|$ for a fixed channel i, obtained using the dimensional regularisation scheme to compute the loop function. The vertical dashed lines represent the location of the thresholds of the different channels.

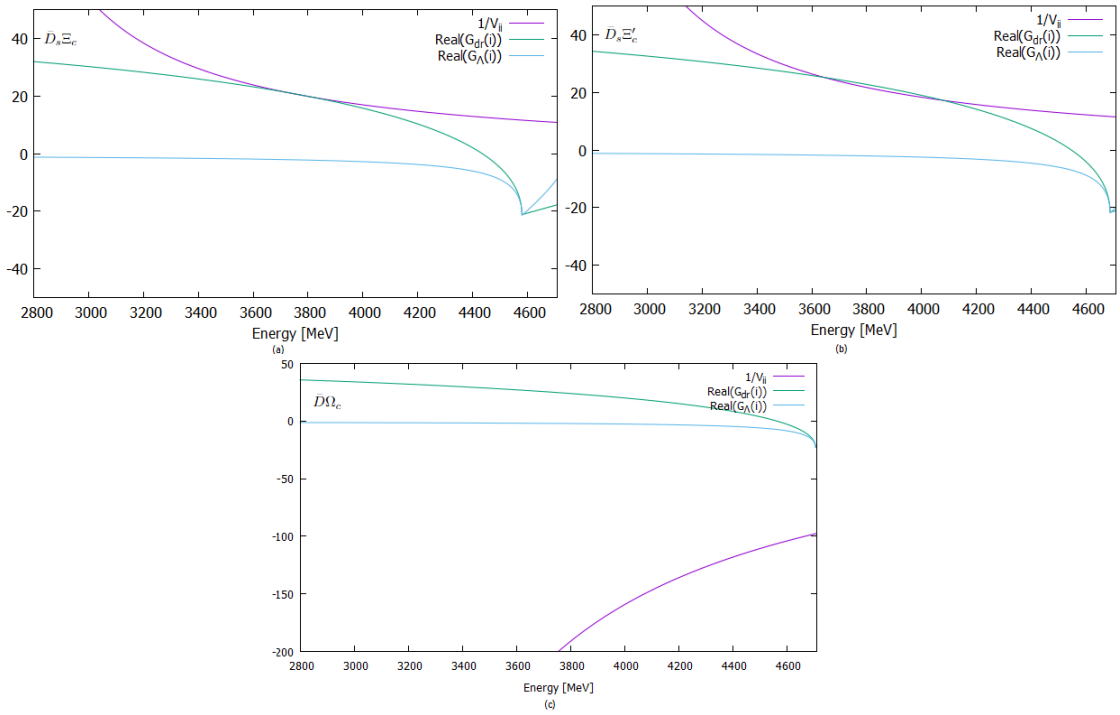

Fig. 20: The purple line represents the inverse of the diagonal term of the potential, the green line shows the loop function of the same channel, computed using a dimensional regularisation scheme and the blue line is similar to the green one but computed using a cut-off scheme. In (a) we have the $\bar{D}_s^*\Xi_c$ channel, in (b) the $\bar{D}_s^*\Xi_c'$ and in (c) the $\bar{D}^*\Omega_c$

This state is not found in Ref. [10],for the same as in PB sector, namely the assumption of a null coefficient for the diagonal potential including the exchange of a very massive $c\bar{c}$ meson. In our case we have a small coefficient, κ_{cc}, which permits the action of coupled channels to take place. We can check that this state is produced due to the large value of C_{89}, similar to how we proceeded in the PB sector. We change $C_{89} \to C'_{89} = \gamma C_{89}$, adding the gamma factor, and then we study how the resonance is generated for different values of gamma. The results are displayed in Fig. 22, where we can clearly see that it is the cross term, including the coupled channel effect, the responsible for producing dynamically generated resonances. There we can clearly see the effect of

$1^- \oplus \frac{1}{2}^+$ interaction in the $(I,S)=(0,-2)$ sector				
M(Mev)		4633.38		
Γ(MeV)		79.58		
	Λ	g	$\lvert g_i\rvert$	χ_i
$J/\psi\Xi(4415)$	800	$-1.62+0.38i$	1.66	0.252
$\bar{D}_s^*\Xi_c(4581)$	800	$-0.143+0.32i$	0.34	0.022
$\bar{D}_s^*\Xi_c'(4689)$	800	$-2.49+0.67i$	2.58	0.406
$\bar{D}^*\Omega_c(4706)$	800	$3.67+0.89i$	3.78	0.740

Table 7: Position, cut off, couplings and compositeness of the Ξ states generated with the light channels of the PB interaction.

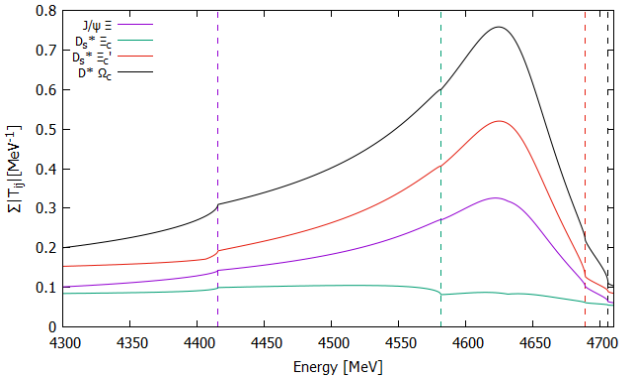

Fig. 21: Solid lines represent the sum over all j channels of the modulus of the VB scattering amplitude, $|T_{ij}|$ for a fixed channel i, obtained using the cut-off scheme to compute the loop function. The vertical dashed lines represent the location of the thresholds of the different channels.

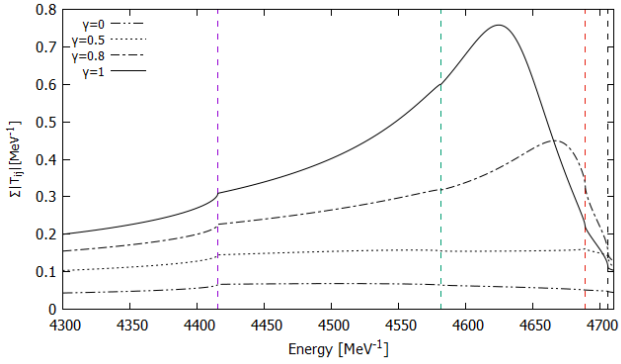

Fig. 22: Solid lines represent the sum over all j channels of the modulus of the PB scattering amplitude, $|T_{ij}|$ for $i=\bar{D}^*\Omega_c$, obtained using the cut-off scheme to compute the loop function. The vertical dashed lines represent the location of the thresholds of the different channels.

the cross term is the reason why the resonances is dynamically generated.

3.2 Exotic hadrons in $\Xi_b \to \Xi\ J/\psi\ \phi$ decay

3.2.1 The $J/\psi\ \phi$ mass distribution

We start studying the $J/\psi\ \phi$ mass distribution, which will allow us to see the $X(4140)/X(4160)$ interplay. As it was discussed in section 1. we consider two possibles models, one which is based in the latest experimental results (Refs. [23, 36]) where is proposed there exists a board $X(4140)$

resonance with a pole position of $M_R = 4146.5$ MeV and a width of $\Gamma = 83$ MeV and another model, which assumes the existence of a narrow $X(4140)$ plus a wide $X(4160)$ resonance, which come from earlier experimental results [10–14] and recent theoretical results [33].

We start with the model with a wide $X(4140)$, the corresponding results are sown in Fig. 23, where we can see the $J/\psi\phi$ invariant mass distribution for the tree level calculations (Fig. 6), and the corresponding spectrum when we also take into account the FSI (Figs. 8). As we can see the effect of the FSI is rather small.This will be also true for the model with two X resonances, so in this section we will further present only the results that include the FSI.

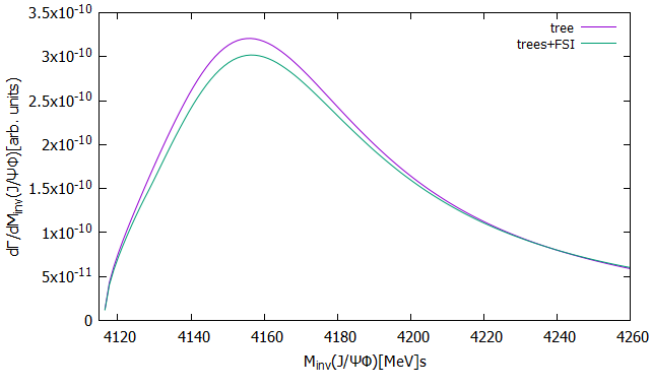

Fig. 23: The J/ψ ϕ mass spectrum computed using one wide $X(4140)$ resonance. The green line corresponds to tree level calculations only, while the purple one to whose with the FSI effects.

Once seen the results for the one resonance model we are going to discuss the results generated with two resonances, where similarly to the results to Ref. [32] we adjust β to a value which generates two X resonances of a similar strength. The pole position for the $X(4140)$ resonance is $M_R = 4132$ MeV and a width of $\Gamma = 19$ MeV, while the $X(4160)$ can be generated as $D_s^* \bar{D}_s^*$ molecule, as we explained in the section 2.2.1. The corresponding model contains a loop-function that diverges and must be regularised. In ref [27] this loop function is regularised using a dimensional regularisation method, but as we proved earlier such a scheme can produce fake poles, so in this work we use the cut-off regularisation method with $\Lambda = 650$ MeV, which reproduces the results obtained using the dimensional regularisation from [27].

The J/ψ ϕ invariant mass distribution for two X resonances can be seen in Fig. 24. Where we can see a narrow $X(4140)$ peak at 4132 MeV, and a rather wide $X(4160)$ peak. Note that $X(4160)$ also produces a cusp around 4224 MeV, which corresponds to the $D_s^* \bar{D}_s^*$ threshold. As it is mentioned in ref. [32], if this cusp is experimentally detected it would strongly suggest a molecular interpretation of $X(4160)$ as well as the existence of narrow $X(4140)$ and wide $X(4160)$ resonances.

We also would like to analyse the sensibility of the obtained distribution with respect to the parameter β, and for this purpose we generated similar spectra for different values of β. As it can be seen in Fig. 25 the effect of changing the value of β effects mainly to the height of the $X(4140)$ peak but, it is also important to note that for large values of β the cusp at the threshold of $D_s^* \bar{D}_s^*$ starts to disappear.

3.2.2 The J/ψ Ξ mass distribution

Now we discuss the results for the J/ψ Ξ mass distribution, which is the channel where we expect to see the signature of the $S = -2$ pentaquark. The properties of the pentaquark dynamically generated by our heavy channel model are presented in Tab. 7. This state has a mass $M_R = 4633.38$ MeV, and a width $\Gamma_R = 79.58$ MeV, and rather strongly couples to $J/\psi\Xi$ channel,coupling constant is $g_{J/\phi\Xi} = -1.62 + 0.38i$. We will take these values for the pole position and

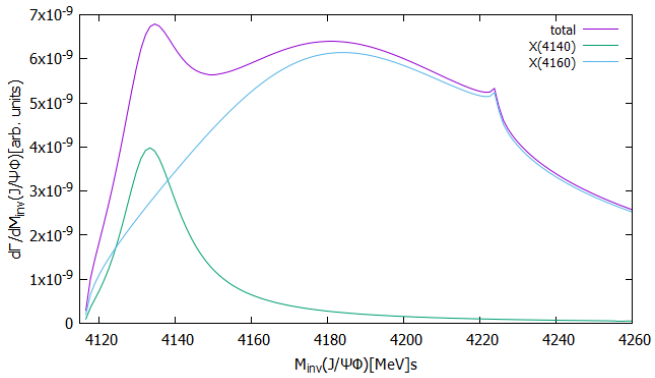

Fig. 24: The purple line represents the J/ψ ϕ mass spectrum generated using two resonance model. The green and the blue lines show the individual contributions from $X(4140)$ and $X(4160)$, respectively. The parameter β, Eq. 35, is taken as $\beta = \beta_0/2.6$, where β_0 is the value taken in Ref. [33]

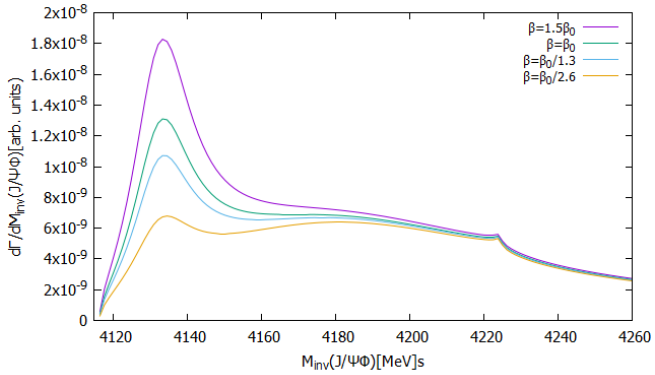

Fig. 25: The solid lines represent the J/ψ ϕ mass spectrum generated using the $X(4140)$ and the $X(4160)$ resonances for different values of the weight factor β, which controls the relative contributions of the two resonances; β_0 is the value of β given in Ref. [33]

coupling as nominal ones and we will vary them within a reasonable range to explore the sensitivity of our results with respect to the pentaquark parameters.

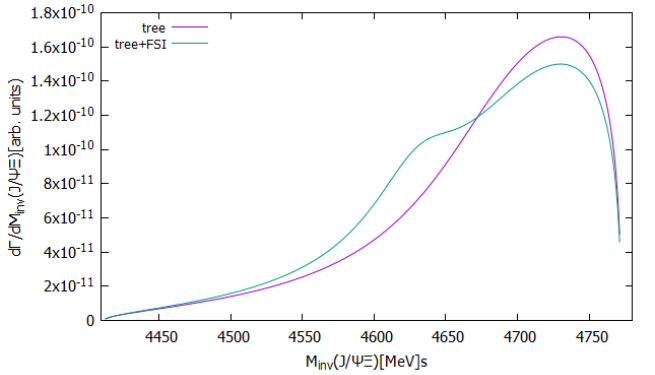

Fig. 26: The J/ψ Ξ spectrum, where the purple line corresponds to the tree level diagram and the green one is obtained also taking into account the final state interactions that generates the $S = -2$ pentaquark.

In this section we proceed in a similar manner as in a previous section, and start with the results computed with one wide $X(4140)$ resonance. In Fig. 26 we can see the $J/\psi\ \Xi$ spectrum, where the purple line is obtained only using the tree-level diagram, while for the green line we have also included the FSI effects. In this latter curve we should see the signal of the $S = -2$ pentaquark, generated in the $J/\psi\ \Xi$ interaction. First of all as seen in Fig. 26, the background shows itself a peak structure around 4730 MeV. While the effect of the pentaquark is the appearance of a bump around the nominal pentaquark mass of 4633 MeV that could be detected. Note that the pentaquark interferes with the background positively, and even being a wide resonance it has an important effect on the spectrum due to it strong coupling with the $J/\psi\Xi$ channel.

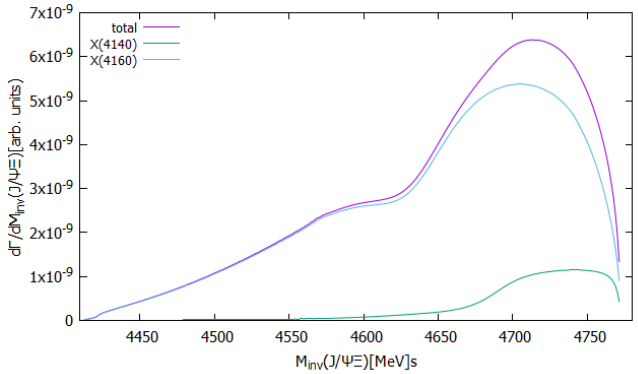

Fig. 27: The purple line represents the $J/\psi\ \Xi$ spectrum computed with a narrow $X(4140)$ plus a $X(4160)$, while the green and the blue ones show the individual contribution from the $X(4140)$ and the $X(4160)$, respectively.

Let's now consider the calculation with a narrow $X(4140)$ and a $X(4160)$ resonances. The results (with FSI) can be seen in Fig. 27, where the green and the blue curves show the individual contribution of the $X(4140)$ and the $X(4160)$ resonances respectively, while the purple curve is the sum of both contributions. Note that the $X(4160)$ contribution is dominant with respect to that of the $X(4140)$. It is also important to see that in contrast to the previous case the pentaquark's signal interferes negatively with the background. This can be seen more clearly in Fig. 28, where we compare the compare the contributions from one and two resonance models with FSI, varying the mass of the pentaquark and its coupling to the $J/\psi\ \Xi$ channel. We do that since we know there can exist some theoretical uncertainties, so we modify the pentaquark pole position by ± 50 MeV and we allow for a 20% of variation of the coupling of the pentaquark to the channel $J/\psi\Xi$. The results presented in Fig. 28 clearly shows that in all cases the presence of the double strangeness pentaquark is experimentally detectable. Actually in the case of one wide $X(4140)$ this task seems to be much simpler. And certainly the experimental measurement of the $J/\psi\Xi$ invariant mass spectrum form $\Xi_b \to \Xi\ J/\psi\ \phi$ decay would also allow to distinguish between one wide $X(4140)$ or two X models.

3.2.3 The $\phi\ \Xi$ mass distribution

Finally we present the results for the $\phi\ \Xi$ invariant mass distribution where we expect to see the signal of the $\Xi(2500)$. This state appear in PDG [35] as a one-star state, with a mass $M_{\Xi(2500)} = 2500$ MeV and there exist two experimental groups that reported different values for its width, which are 150 [37] and 50 MeV [38]. Based on this information we decided to generate the spectrum for tree different cases $\Gamma = 50,\ 100,\ 150$ MeV. We neither know which is the coupling of this state to the $\phi\Xi$ channel, therefore we explore the range of values of this coupling, which would allow to see the signal of $\Xi(2500)$ in generated spectrum

The corresponding results are the presented in Fig. 29. The value of the coupling constant, needed to generate a significant interference with the background, as we could expect, is larger if

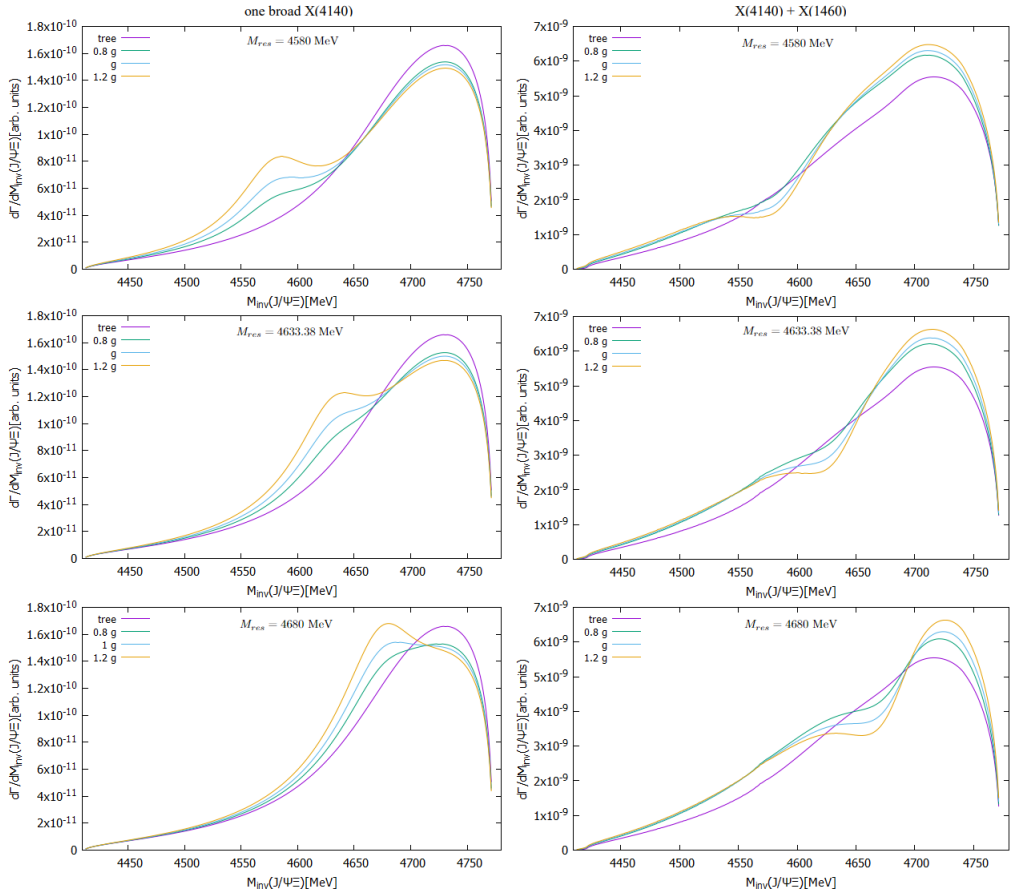

Fig. 28: J/ψ Ξ spectrum computed with one broad $X(4140)$ resonance (left panels) or with a narrow $X(4140)$ plus a $X(4160)$ state (right panels) with different values of the $g_{J/\psi\Xi}$ coupling and different pole positions for the resonance [4580 MeV (top), 4663.38 MeV (middle) and 4680 MeV (bottom)]

the state has a larger width. We can see that if $\Gamma = 50$ MeV then the minimum absolute value of the coupling is around 0.7, while for a $\Xi(2500)$ with $\Gamma = 150$ MeV this value it is around $1.7 - 1.9$. Similarly to the previous case the interference of the resonance with the background is positive for the case of one wide $X(4140)$ resonance, while for the case of a narrow $X(4140)$ and $X(4160)$ resonances the interference is negative. Thus, we see that studying this spectrum would we also very interesting if the coupling of $\Xi(2500)$ is large enough.

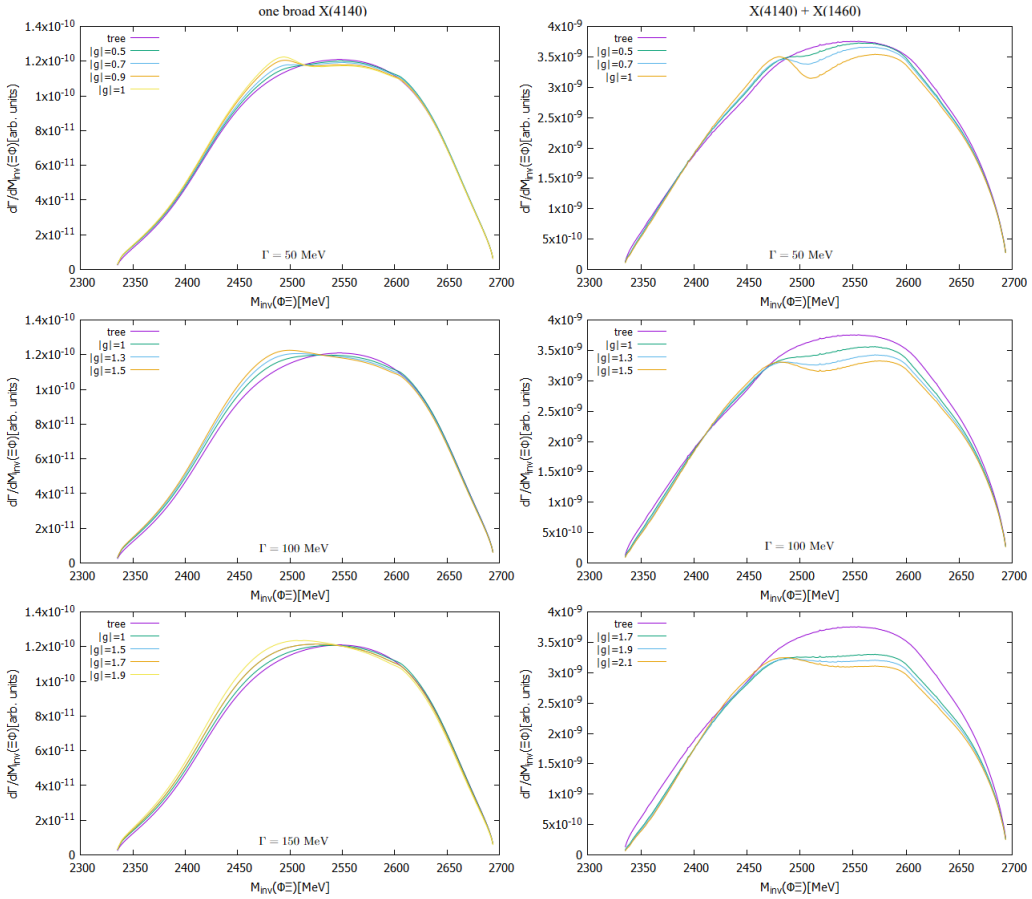

Fig. 29: The $\phi\ \Xi$ spectrum computed with one broad $X(4140)$ resonance (left panels) or with narrow $X(4140)$ plus a $X(4160)$ states (right panels) with different values for the coupling of the $\Xi(2500)$ to the $\phi\ \Xi$ channel, and different widths of the resonance [50 MeV (top), 100 MeV (middle) and 150 MeV (bottom)]

4. Conclusions

The discovery in the last years of many exotic hadrons not fitting into the conventional quark composition model, has converted this topic into an important field of research. Motivated by this fact, in the present work we studied some resonances that could be interpreted as quasi-bound states of an interacting meson-baryon pair in the strangeness -2 and isospin $1/2$ sector, employing effective Lagrangians for describing the exchange of a vector meson in the t-channel. We also proposed a decay process ($\Xi_b \to \Xi\ J/\psi\ \phi$) suitable to detect some of those exotic hadrons in all two-particle channels.

First of all, in this work we find two poles, which can be associated to the $\Xi(1620)$ and $\Xi(1690)$ resonances from PDG [35] in the scattering amplitude of the interaction of pseudoscalar mesons with baryons in the light-channel sector. By modifying some parameters parameters in a reasonable range we can reproduce the experimental masses of the $\Xi(1620)$ and $\Xi(1690)$, producing two states at 1600 MeV and 1685.40 MeV. With this result we can conclude that the $\Xi(1620)$ and $\Xi(1690)$ may have meson-baryon molecular origin, where the $\Xi(1620)$ has an important $\pi\Xi$ component, around 50%, with a mixture of 20% of $\bar{K}\Lambda$. The $\Xi(1690)$ is mainly a $\bar{K}\Sigma$ molecule with a small component (2%) of $\eta\Xi$. Both of these resonances have well defined spin-parity ($J^\pi = \frac{1}{2}^-$) since they are generated from the interaction of a pseudoscalar meson ($J^\pi = 0^-$) and an octet baryon ($J^\pi = \frac{1}{2}^-$) in s-wave. A measurement of the spin-parity of these states could confirm or refuse this hypothesis

For the light-channel sector of the vector meson baryon interaction we can also find two resonances in the scattering amplitude, which could be associated with two states listed in the PDG, namely the $\Xi(1820)$ and $\Xi(1950)$ [35]. Similarly to what we did in the PB section, by modifying some parameters we can bring positions of these two states closer to their experimental mass, but the theoretical widths are much smaller than the experimental ones. This might be solved allowing the coupling between the vector mesons with the pseudoscalar mesons and thus opening decays to lighter channels and correspondingly increasing the width of the states dynamically generated in our work. If this approach is assumed to represent the nature of these states, we could understand the $\Xi(1820)$ as a mixture of $\phi\Xi$ (33%) and $\bar{K}^*\Lambda$ (13%) components, while the $\Xi(1950)$ would be a mixture of $\bar{K}^*\Sigma$ (50%), $\omega\Xi$ (10%) and $\phi\Xi$ (10%) one. Note that these states are degenerate in spin-parity and form a $J^\pi = \frac{1}{2}^-$, $J^\pi = \frac{3}{2}^-$ doublet. This would be compatible with the quantum numbers of the $\Xi(1820)$, which are $J^\pi = \frac{3}{2}^-$.

Another solution would be to generate the two resonances in the region of the $\Xi(1950)$, producing an apparent wide resonance. This is a possibility mentioned in the PDG, where it is said that the $\Xi(1950)$ may be more than one Ξ state.

We have also shown that it is important to take care of the fake poles that are generated in regions where the potential is repulsive. These fake poles appeared in the heavy sector if we are using a dimensional regularisation scheme to re-normalise the loop function and we avoided the problem by using a cut-off scheme to compute the loop function. The results for the heavy channels are quite encouraging, as they point forwards the existence of doubly strangeness pentaquarks with hidden charm, which can be generated thanks to the coupled-channel structure of our model.

In the pseudoscalar meson baryon interaction sector we can generate one hidden charm $S = -2$ baryon with $M = 4493$ MeV and $\Gamma = 73$ MeV, which can be interpret as a $\bar{D}\Omega_c$ molecule, and the quantum numbers of this state would be $J^\pi = \frac{1}{2}^-$. In the vector meson baryon interaction sector we can also generate one state with $M = 4633$ MeV and $\Gamma = 79$ MeV and, similarly to the previous case, this state can be understood as a $\bar{D}^*\Omega_c$ molecule which would be degenerate in spin-parity forming a $J^\pi = \frac{1}{2}^-$, $J^\pi = \frac{3}{2}^-$ doublet.

The main motivation to study the $\Xi_b \to \Xi\ J/\psi\ \phi$ decay came form the Dalitz plots of Fig. 1, which proved the potential possibility to study several exotic states that may be detected in all three two-body invariant mass spectra.Similarly to what is done in [32] we develop two different models for the interpretation of the $X(4140)$ and $X(4160)$ resonances. The first model considers that there only exists one wide $X(4140)$ state while the other claims the existence of a narrow $X(4140)$ resonance plus a $X(4160)$ one.Consequent in the $J/\psi\phi$ mass spectrum, due to the nature of the $X(4160)$ as a $D_s^*\bar{D}_s^*$ [27] bound system, there appears a cusp near the threshold of this channel (4224 MeV). Therefore, if this cusp is detected, it would be a clear signal that the two-resonances model is the one that represents the nature of the X resonances, and also that $X(4160)$ is a molecular state.

The $X(4274)$, $X(4350)$ and the $X(4500)$ resonances may also leave a signal at higher J/ψ invariant masses in the $\Xi_b \to \Xi\ J/\psi\ \phi$ decay, but in this work these states where not included as we do not have a theoretical model that generates them.

In the $J/\psi\Xi$ spectrum, we studied the possibility of detecting the doubly strange pentaquark with hidden charm, which we introduce as Breit-Wigner, using the parameters obtained from the coupled channel approach developed in this work in section 3.1.2. This permit us to keep the model simple and do variations on the parameters easily. The results are very promising, since if the mass of this state lies in the region $4580 - 4680$ MeV it has a good chance to be experimentally detected. We have also shown that in the case of a single wide $X(4140)$ model the pentaquark signal interferes positively with the background, while fr the two X model this interference is negative. This potentially allows to differentiate between these two situations one the corresponding

spectrum will be measured.

Finally we also studied the $\phi\Xi$ spectrum, where we explored the possibility to detect the $\Xi(2500)$. For this resonance there exists a discussion about whether its width is 50 MeV or 150 MeV [35], so we studied these two possibilities plus an intermediate case of $\Gamma = 100$ MeV. Our results presented in section 3.2.3 allows us to conclude that if the resonance has a narrow width of 50 MeV, even with small coupling ($g_{\phi\Xi} \sim 0.7 - 0.9$) its signal in the spectrum has high chances to be detected, whereas if $\Gamma = 100$ MeV the coupling should be bigger than $g_{\phi\Xi} = 1.3$, and in the case $\Gamma = 150$ MeV the value of the coupling has to be bigger than $g_{\phi\Xi} = 1.9$ in order to produce a significant signal above the background.

A Appendix A: Double loop integral

In our discussion of the $\Xi_b \to \Xi\ J/\psi\ \phi$ decay we gave the expression for two final state interaction amplitudes $\mathcal{M}^{J/\psi\Xi}_{4160}$, and $\mathcal{M}^{\phi\Xi}_{4160}$ which involve a loop integral that is a 3-vector. In this appendix we demonstrate how we arrive to those two expressions. Similarly we will derive the expressions for the $\mathcal{M}^{J/\psi\Xi}_{4140}$, and $\mathcal{M}^{\phi\Xi}_{4140}$ amplitudes.

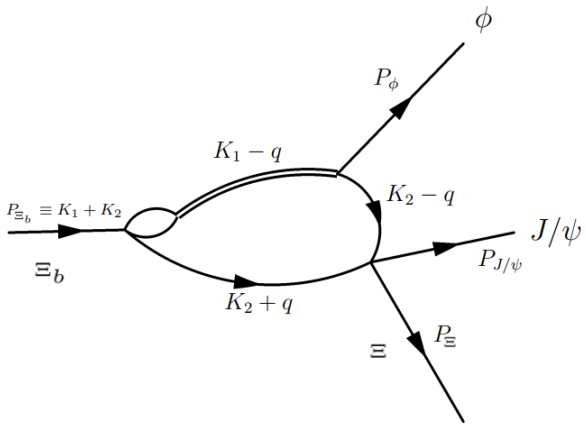

Fig. 30: Feynman diagram associated to the $\mathcal{M}^{J/\psi\Xi}_{4160}$ amplitude, where we show the corresponding momenta for all the particle lines.

In Fig. 30 we can see the the diagram associated to the $\mathcal{M}^{J/\psi\Xi}_{4160}$, where the momenta of each particle is shown. From this diagram we can write the full expression of the $\mathcal{M}^{J/\psi\Xi}_{4160}$ amplitude, being:

$$\mathcal{M}^{J/\psi\Xi}_{4160} = iT_{J/\psi\Xi,J/\psi\Xi}\int \frac{d^4q}{(2\pi)^4}\frac{(\vec{\epsilon}_{J/\psi}\times\vec{\epsilon}_\phi)\cdot(\vec{K}_2+\vec{q})G_{D_s^*\bar{D}_s^*}}{(K_1-q)^2-M_X^2+iM_X\Gamma_X} \frac{1}{(K_2-q)^2-M^2_{J/\psi}+i\epsilon}\frac{2M_\Xi}{(K_2+q)^2-M^2_\Xi+i\epsilon}, \tag{41}$$

where $\vec{K}_1 = (\vec{P}_\Xi + \vec{P}_\phi)/2$ and $\vec{K}_2 = (\vec{P}_\Xi - \vec{P}_\phi)/2$. $T_{J/\psi\Xi,J/\psi\Xi}$ denotes the scttering amplitude for the corresponding channels, which we introduce as a Breit-Wigner with the $S=-2$ pentaquark parameters. As it is discussed in section 2.2.2 the $J/\psi\ \phi$ interaction has to be in P-wave what leads to appearance of the vector product of the corresponding polarisation vectors. Finally, the three propagators are the ones corresponding to the three internal lines for the J/ψ, Ξ and $X(4160)$ resonance. From this expression we can separate the q^0 component and rearrange some terms in order simplify it, obtaining that

$$\mathcal{M}^{J/\psi\Xi}_{4160} = iT_{J/\psi\Xi,J/\psi\Xi}(\vec{\epsilon}_{J/\psi}\times\vec{\epsilon}_\phi)\int\frac{d^3q}{(2\pi)^3}(\vec{K}_2+\vec{q})\int\frac{dq^0}{2\pi}\frac{G_{D_s^*\bar{D}_s^*}}{(K_1^0-q^0)^2-\omega_X^2+iM_X\Gamma_X} \frac{1}{(K_2^0-q^0)^2-\omega^2_{J/\psi}+i\epsilon}\frac{2M_\Xi}{(K_2^0+q^0)^2-\omega^2_\Xi+i\epsilon}, \tag{42}$$

where $\omega_X = M_X + (\vec{K}_1 - \vec{q}))^2$, $\omega_{J/\psi} = M_{J/\psi} + (\vec{K}_2 - \vec{q}))^2$ and $\omega_\Xi = M_\Xi + (\vec{K}_2 + \vec{q}))^2$. If we take a non relativistic limit this expression can be written like this,

$$\mathcal{M}^{J/\psi\Xi}_{4160} = iT_{J/\psi\Xi,J/\psi\Xi}(\vec{\epsilon}_{J/\psi}\times\vec{\epsilon}_\phi)\int\frac{d^3q}{(2\pi)^3}(\vec{K}_2+\vec{q})\int\frac{dq^0}{2\pi}\frac{G_{D_s^*\bar{D}_s^*}}{2\omega_X[K_1^0-q^0-\omega_X+i\frac{\Gamma_X}{2}} \frac{1}{2\omega_{J/\psi}[K_2^0-q^0-\omega_{J/\psi}+i\epsilon]}\frac{M_\Xi}{\omega_\Xi[K_2^0+q^0-\omega_\Xi+i\epsilon]}. \tag{43}$$

From this expression we can now clearly see where are the poles of this integral, which are

$$q^0 = K_1^0 - \omega_X + i\frac{\Gamma}{2} \qquad \text{Resonance}, \tag{44}$$

$$q^0 = K_2^0 - \omega_{J/\psi} + i\epsilon \quad \text{J}/\psi \text{ propagator}, \tag{45}$$

$$q^0 = -K_2^0 + \omega_\Xi - i\epsilon \qquad \Xi \text{ propagator}. \tag{46}$$

Since we have two poles adobe the real axis and one below, we compute the integral using the contour integration method choosing to close the contour in the lower half plane. Thus we only piking the Ξ propagator pole, finding

$$\mathcal{M}_{4160}^{J/\psi\Xi} = T_{J/\psi\Xi,J/\psi\Xi}(\vec{\epsilon}_{J/\psi}\times\vec{\epsilon}_\phi)\int\frac{d^3q}{(2\pi)^3}\frac{(\vec{K}_2+\vec{q})G_{D_s^*\bar{D}_s^*}}{2\omega_X[K_1^0+K_2^0-\omega_\Xi-\omega_X+i\frac{\Gamma_X}{2}]}\frac{1}{2\omega_{J/\psi}[2K_2^0-\omega_\Xi-\omega_{J/\psi}+i\epsilon]}\frac{M_\Xi}{\omega_\Xi}. \tag{47}$$

To compute this integral we work in the Jackson frame (the J/ψ ϕ rest frame), where the $\vec{K}_1$ and $\vec{K}_2$ are almost equal since, P_ϕ is small. So we can can replace $\vec{K}_1$ with $\vec{K}_2$, and thus now the integral only depends on $\vec{K}_2$. So we can take the integral to be proportional to this vector, giving us

$$\mathcal{M}_{4160}^{J/\psi\Xi} = T_{J/\psi\Xi,J/\psi\Xi}(\vec{\epsilon}_{J/\psi}\times\vec{\epsilon}_\phi)\vec{K}_2 I_{X(4160)}^{J/\psi\Xi}, \tag{48}$$

with,

$$I_{X(4160)}^{J/\psi\Xi} = \int\frac{d^3q}{(2\pi)^3}\frac{\vec{K}_2\cdot\vec{q}\,G_{D_s^*\bar{D}_s^*}}{2\omega_X[K_1^0+K_2^0-\omega_\Xi-\omega_X+i\frac{\Gamma_X}{2}]}\frac{1}{|\vec{K}_2|^2}\frac{1}{2\omega_{J/\psi}[2K_2^0-\omega_\Xi-\omega_{J/\psi}+i\epsilon]}\frac{M_\Xi}{\omega_\Xi}, \tag{49}$$

where we made the shift $\vec{q}\to\vec{q}+\vec{K}_2$, and $\omega_X = M_X^2+(2\vec{K}_2-\vec{q})^2$, $\omega_{J/\psi} = M_{J/\psi}^2+(2\vec{K}_2-\vec{q})^2$ and $\omega_\Xi = M_\Xi^2+\vec{K}_2^2$.

Once we have $\mathcal{M}_{4160}^{J/\psi\Xi}$, to evaluate the $\mathcal{M}_{4160}^{\phi\Xi}$ is rather straightforward, as we only need to change J/ψ to ϕ and vice versa. In the Jackson frame this is equal to interchange of $\vec{K}_2$ and $\vec{K}_1$, leading us to

$$\mathcal{M}_{4160}^{\phi\Xi} = T_{\phi\Xi,\phi\Xi}(\vec{\epsilon}_{J/\psi}\times\vec{\epsilon}_\phi)\vec{K}_1 I_{X(4160)}^{\phi\Xi}, \tag{50}$$

with,

$$I_{X(4160)}^{\phi\Xi} = \int\frac{d^3q}{(2\pi)^3}\frac{\vec{K}_1\cdot\vec{q}\,G_{D_s^*\bar{D}_s^*}}{2\omega_X[K_1^0+K_2^0-\omega_\Xi-\omega_X+i\frac{\Gamma_X}{2}]}\frac{1}{|\vec{K}_1|^2}\frac{1}{2\omega_\phi[2K_1^0-\omega_\Xi-\omega_\phi+i\epsilon]}\frac{M_\Xi}{\omega_\Xi}, \tag{51}$$

where $\omega_X = M_X^2+(2\vec{K}_1-\vec{q})^2$, $\omega_\phi = M_\phi^2+(2\vec{K}_1-\vec{q})^2$ and $\omega_\Xi = M_\Xi^2+\vec{K}_1^2$.

Finally we can also deviate the expressions for $\mathcal{M}_{4140}^{J/\psi\Xi}$, and $\mathcal{M}_{4140}^{\phi\Xi}$ proceeding in an analogous way with the difference that now we do not have the $G_{D_s^*\bar{D}_s^*}$ loop-function and all interaction are in S-wave, and consequently these amplitudes are scalars.

$$\mathcal{M}_{4140}^{J/\psi\Xi} = T_{J/\psi\Xi,J/\psi\Xi} I_{X(4140)}^{J/\psi\Xi}, \tag{52}$$

with,

$$I_{X(4140)}^{J/\psi\Xi} = \int\frac{d^3q}{(2\pi)^3}\frac{1}{2\omega_X[K_1^0+K_2^0-\omega_\Xi-\omega_X+i\frac{\Gamma_X}{2}]}\frac{1}{2\omega_{J/\psi}[2K_2^0-\omega_\Xi-\omega_{J/\psi}+i\epsilon]}\frac{M_\Xi}{\omega_\Xi}, \tag{53}$$

where $\omega_X = M_X^2 + (2\vec{K}_2 - \vec{q})^2$, $\omega_{J/\psi} = M_{J/\psi}^2 + (2\vec{K}_2 - \vec{q})^2$ and $\omega_\Xi = M_\Xi^2 + \vec{K}_2^2$, and

$$\mathcal{M}_{4140}^{\phi\Xi} = T_{\phi\Xi,\phi\Xi} I_{X(4140)}^{\phi\Xi}, \tag{54}$$

with,

$$I_{X(4140)}^{\phi\Xi} = \int \frac{d^3q}{(2\pi)^3} \frac{1}{2\omega_X[K_1^0 + K_2^0 - \omega_\Xi - \omega_X + i\frac{\Gamma_X}{2}]} \frac{1}{2\omega_\phi[2K_1^0 - \omega_\Xi - \omega_\phi + i\epsilon]} \frac{M_\Xi}{\omega_\Xi}, \tag{55}$$

where $\omega_X = M_X^2 + (2\vec{K}_1 - \vec{q})^2$, $\omega_\phi = M_\phi^2 + (2\vec{K}_1 - \vec{q})^2$ and $\omega_\Xi = M_\Xi^2 + \vec{K}_1^2$.

B Appendix B: Spin Sums

During our discussion of the $\Xi_b \to \Xi\ J/\psi\ \phi$ decay we needed to compute the $\overline{|\mathcal{M}|^2}$. In this appendix we show in more details how we arrived to our final result, Eq. (39). So we start with $\mathcal{M}_4160$ amplitude in the following form:

$$\mathcal{M}_{4160} = (\vec{\epsilon}_{J/\psi} \times \vec{\epsilon}_\phi) \cdot (\vec{P}_\Xi \tilde{\mathcal{M}}_{4160}^P + \vec{K}_2 \tilde{\mathcal{M}}_{4160}^{J/\psi} + \vec{K}_1 \tilde{\mathcal{M}}_{4160}^\phi), \tag{56}$$

where $\vec{K}_1 = (\vec{P}_\Xi + \vec{P}_\phi)/2$ and $\vec{K}_2 = (\vec{P}_\Xi - \vec{P}_\phi)/2$. Now we take the square of the absolute value of $\mathcal{M}_{4160}$,

$$|\mathcal{M}_{4160}|^2 = \varepsilon^{ijk}\epsilon_{J/\psi}^j \epsilon_\phi^k \varepsilon^{abc} \epsilon_{J/\psi}^b \epsilon_\phi^c (P_\Xi^i \tilde{\mathcal{M}}_{4160}^P + K_2^i \tilde{\mathcal{M}}_{4160}^{J/\psi} + K_1^i \tilde{\mathcal{M}}_{4160}^\phi) \cdot (P_\Xi^a \tilde{\mathcal{M}}_{4160}^{*P} + K_2^a \tilde{\mathcal{M}}_{4160}^{*J/\psi} + K_1^a \tilde{\mathcal{M}}_{4160}^{*\phi}), \tag{57}$$

where ε is the Levi-Civita symbol.

Note that since we are working in a reference frame where $J/\psi\ \phi$ system is in rest, the 3-momenta of all these particles are small in comparison with their masses, therefore we can take a non-relativistic limit, where

$$\sum_{pol} \epsilon_{J/\psi}^j \epsilon_{J/\psi}^b = \delta^{jb}, \tag{58}$$

$$\sum_{pol} \epsilon_\phi^k \epsilon_\phi^c b = \delta^{kc}. \tag{59}$$

Hence performing the sum over the polarisations the Eq. (57) can be simplified to:

$$\overline{|\mathcal{M}_{4160}|^2} = \varepsilon^{ijk}\varepsilon^{ajk} (P_\Xi^i \tilde{\mathcal{M}}_{4160}^P + K_2^i \tilde{\mathcal{M}}_{4160}^{J/\psi} + K_1^i \tilde{\mathcal{M}}_{4160}^\phi) \cdot (P_\Xi^a \tilde{\mathcal{M}}_{4160}^{*P} + K_2^a \tilde{\mathcal{M}}_{4160}^{*J/\psi} + K_1^a \tilde{\mathcal{M}}_{4160}^{*\phi}). \tag{60}$$

Now, applying the $\varepsilon^{ijk}\varepsilon^{ajk} = \delta^{ia}$ property we obtain that:

$$\overline{|\mathcal{M}_{4160}|^2} = (\vec{P}_\Xi \tilde{\mathcal{M}}_{4160}^P + \vec{K}_2 \tilde{\mathcal{M}}_{4160}^{J/\psi} + \vec{K}_1 \tilde{\mathcal{M}}_{4160}^\phi) \cdot (\vec{P}_\Xi \tilde{\mathcal{M}}_{4160}^{*P} + \vec{K}_2 \tilde{\mathcal{M}}_{4160}^{*J/\psi} + \vec{K}_1 \tilde{\mathcal{M}}_{4160}^{*\phi}). \tag{61}$$

From this expression we can straightforward derive the Eq. (39) just by computing the scalar products.

References

[1] R. H. Dalitz and S. F. Tuan, Annals Phys. **10**, 307-351 (1960) doi:10.1016/0003-4916(60)90001-4

[2] N. Kaiser, P. B. Siegel and W. Weise, Nucl. Phys. A **594**, 325-345 (1995) doi:10.1016/0375-9474(95)00362-5 [arXiv:nucl-th/9505043 [nucl-th]].

[3] E. Oset and A. Ramos, Nucl. Phys. A **635**, 99-120 (1998) doi:10.1016/S0375-9474(98)00170-5 [arXiv:nucl-th/9711022 [nucl-th]].

[4] J. A. Oller and E. Oset, Nucl. Phys. A **620**, 438-456 (1997) [erratum: Nucl. Phys. A **652**, 407-409 (1999)] doi:10.1016/S0375-9474(97)00160-7 [arXiv:hep-ph/9702314 [hep-ph]].

[5] J. A. Oller, E. Oset and J. R. Pelaez, Phys. Rev. D **59**, 074001 (1999) [erratum: Phys. Rev. D **60**, 099906 (1999); erratum: Phys. Rev. D **75**, 099903 (2007)] doi:10.1103/PhysRevD.59.074001 [arXiv:hep-ph/9804209 [hep-ph]].

[6] J. R. Pelaez, Phys. Rept. **658**, 1 (2016) doi:10.1016/j.physrep.2016.09.001 [arXiv:1510.00653 [hep-ph]].

[7] R. Aaij *et al.* [LHCb], Phys. Rev. Lett. **115**, 072001 (2015) doi:10.1103/PhysRevLett.115.072001 [arXiv:1507.03414 [hep-ex]].

[8] R. Aaij *et al.* [LHCb], Phys. Rev. Lett. **122**, no.22, 222001 (2019) doi:10.1103/PhysRevLett.122.222001 [arXiv:1904.03947 [hep-ex]].

[9] M. Wang (LHCb Collaboration), Implications Workshop (2020), https://indico.cern.ch/event/857473/timetable/32- exotic-hadrons-experimental.

[10] J. J. Wu, R. Molina, E. Oset and B. S. Zou, Phys. Rev. C **84**, 015202 (2011) doi:10.1103/PhysRevC.84.015202 [arXiv:1011.2399 [nucl-th]].

[11] J. Hofmann and M. F. M. Lutz, Nucl. Phys. A **763**, 90-139 (2005) doi:10.1016/j.nuclphysa.2005.08.022 [arXiv:hep-ph/0507071 [hep-ph]].

[12] S. G. Yuan, K. W. Wei, J. He, H. S. Xu and B. S. Zou, Eur. Phys. J. A **48**, 61 (2012) doi:10.1140/epja/i2012-12061-2 [arXiv:1201.0807 [nucl-th]].

[13] C. W. Xiao, J. Nieves and E. Oset, Phys. Rev. D **88**, 056012 (2013) doi:10.1103/PhysRevD.88.056012 [arXiv:1304.5368 [hep-ph]].

[14] C. Garcia-Recio, J. Nieves, O. Romanets, L. L. Salcedo and L. Tolos, Phys. Rev. D **87**, 074034 (2013) doi:10.1103/PhysRevD.87.074034 [arXiv:1302.6938 [hep-ph]].

[15] F. L. Wang, R. Chen and X. Liu, Phys. Rev. D **103**, no.3, 034014 (2021) doi:10.1103/PhysRevD.103.034014 [arXiv:2011.14296 [hep-ph]].

[16] P. Pakhlov *et al.* [Belle], Phys. Rev. Lett. **100**, 202001 (2008) doi:10.1103/PhysRevLett.100.202001 [arXiv:0708.3812 [hep-ex]].

[17] T. Aaltonen *et al.* [CDF], Phys. Rev. Lett. **102**, 242002 (2009) doi:10.1103/PhysRevLett.102.242002 [arXiv:0903.2229 [hep-ex]].

[18] T. Aaltonen *et al.* [CDF], Mod. Phys. Lett. A **32**, no.26, 1750139 (2017) doi:10.1142/S0217732317501395 [arXiv:1101.6058 [hep-ex]].

[19] R. Aaij *et al.* [LHCb], Phys. Rev. D **85**, 091103 (2012) doi:10.1103/PhysRevD.85.091103 [arXiv:1202.5087 [hep-ex]].

[20] S. Chatrchyan *et al.* [CMS], Phys. Lett. B **734**, 261-281 (2014) doi:10.1016/j.physletb.2014.05.055 [arXiv:1309.6920 [hep-ex]].

[21] V. M. Abazov *et al.* [D0], Phys. Rev. D **89**, no.1, 012004 (2014) doi:10.1103/PhysRevD.89.012004 [arXiv:1309.6580 [hep-ex]].

[22] V. M. Abazov *et al.* [D0], Phys. Rev. Lett. **115**, no.23, 232001 (2015) doi:10.1103/PhysRevLett.115.232001 [arXiv:1508.07846 [hep-ex]].

[23] R. Aaij *et al.* [LHCb], Phys. Rev. Lett. **118**, no.2, 022003 (2017) doi:10.1103/PhysRevLett.118.022003 [arXiv:1606.07895 [hep-ex]].

[24] X. Liu and S. L. Zhu, Phys. Rev. D **80**, 017502 (2009) [erratum: Phys. Rev. D **85**, 019902 (2012)] doi:10.1103/PhysRevD.85.019902 [arXiv:0903.2529 [hep-ph]].

[25] T. Branz, T. Gutsche and V. E. Lyubovitskij, Phys. Rev. D **80**, 054019 (2009) doi:10.1103/PhysRevD.80.054019 [arXiv:0903.5424 [hep-ph]].

[26] X. Chen, X. Lü, R. Shi and X. Guo, [arXiv:1512.06483 [hep-ph]].

[27] R. Molina and E. Oset, Phys. Rev. D **80**, 114013 (2009) doi:10.1103/PhysRevD.80.114013 [arXiv:0907.3043 [hep-ph]].

[28] M. Tanabashi *et al.* [Particle Data Group], Phys. Rev. D **98**, no.3, 030001 (2018) doi:10.1103/PhysRevD.98.030001

[29] J. A. Oller and U. G. Meissner, Phys. Lett. B **500**, 263-272 (2001) doi:10.1016/S0370-2693(01)00078-8 [arXiv:hep-ph/0011146 [hep-ph]].

[30] G. Montaña, A. Feijoo and À. Ramos, Eur. Phys. J. A **54**, no.4, 64 (2018) doi:10.1140/epja/i2018-12498-1 [arXiv:1709.08737 [hep-ph]].

[31] E. Oset and A. Ramos, Eur. Phys. J. A **44**, 445-454 (2010) doi:10.1140/epja/i2010-10957-3 [arXiv:0905.0973 [hep-ph]].

[32] V. Magas, À. Ramos, R. Somasundaram and J. Tena Vidal, Phys. Rev. D **102**, no.5, 054027 (2020) doi:10.1103/PhysRevD.102.054027 [arXiv:2004.01541 [hep-ph]].

[33] E. Wang, J. J. Xie, L. S. Geng and E. Oset, Phys. Rev. D **97**, no.1, 014017 (2018) doi:10.1103/PhysRevD.97.014017 [arXiv:1710.02061 [hep-ph]].

[34] A. Feijoo, V. K. Magas, A. Ramos and E. Oset, Phys. Rev. D **92**, no.7, 076015 (2015) [erratum: Phys. Rev. D **95**, no.3, 039905 (2017)] doi:10.1103/PhysRevD.92.076015 [arXiv:1507.04640 [hep-ph]].

[35] P. A. Zyla *et al.* [Particle Data Group], PTEP **2020**, no.8, 083C01 (2020) doi:10.1093/ptep/ptaa104

[36] R. Aaij *et al.* [LHCb], Phys. Rev. D **95**, no.1, 012002 (2017) doi:10.1103/PhysRevD.95.012002 [arXiv:1606.07898 [hep-ex]].

[37] J. Alitti, V. E. Barnes, E. Flaminio, W. Metzger, D. Radojicic, R. R. Rau, C. R. Richardson, N. P. Samios, D. Bassano and M. Goldberg, *et al.* Phys. Rev. Lett. **22**, 79-82 (1969) doi:10.1103/PhysRevLett.22.79

[38] J. Bartsch *et al.* [Aachen-Berlin-CERN-London-Vienna], Phys. Lett. B **28**, 439-442 (1969) doi:10.1016/0370-2693(69)90346-3

[39] J. J. Wu, R. Molina, E. Oset and B. S. Zou, AIP Conf. Proc. **1374**, no.1, 557-560 (2011) doi:10.1063/1.3647202

[40] A. Ramos, A. Feijoo, Q. Llorens and G. Montaña, Few Body Syst. **61**, no.4, 34 (2020) doi:10.1007/s00601-020-01566-0 [arXiv:2009.04367 [hep-ph]].

[41] F. K. Guo, C. Hanhart, U. G. Meißner, Q. Wang, Q. Zhao and B. S. Zou, Rev. Mod. Phys. **90**, no.1, 015004 (2018) doi:10.1103/RevModPhys.90.015004 [arXiv:1705.00141 [hep-ph]].